Research Article

A Developmental Table for the Florida Carpenter Ant *Camponotus floridanus*: Establishing Foundations for Mechanistic Studies of Development and Evolution in Ants

Travis Chen[1,2], Ab Matteen Rafiqi[2,3], Arjuna Rajakumar[2,4], Nihan Sultan Milat[3,5], Tom Lamouret[2], Érik Plante[2], Benjamin A. Fung[2], Rajendhran Rajakumar[2,6], Ehab Abouheif[1,2]

1. Center for Evolutionary & Organismal Biology, Women's Hospital, School of Medicine, Zhejiang University, China; 2. Department of Biology, McGill University, Canada; 3. Beykoz Institute of Life Sciences and Biotechnology, Bezmialem Vakif University, Turkey; 4. Whitehead Institute for Biomedical Research, Cambridge, United States; 5. Institute of Health Sciences, Bezmialem Vakif University, Turkey; 6. Department of Biology, University of Ottawa, Canada

Developmental staging tables have been essential tools for understanding morphogenesis, gene regulation, and evolutionary change across animal taxa. However, such frameworks are lacking for many species, which are relevant for answering key questions in the fields of ecology, evolutionary, and developmental biology. Here, we present a comprehensive developmental table for the carpenter ant *Camponotus floridanus*, an emerging model system for understanding how ecological environment, eusocial systems, endosymbionts, and organismal development interact and influence each other. Our staging spans embryonic, larval, and pupal development, combining high-resolution and time-lapse imaging to document key events from egg to adult. Stages are defined based on conserved features of insect embryogenesis, including nuclear division, cellularization, gastrulation, germband elongation, segmentation, and dorsal closure. *C. floridanus* has evolved novel, species-specific developmental features, largely driven by its endosymbiosis with the bacteria *Blochmannia*. Despite this, we successfully identified several homologous landmarks that are conserved with those of other ants, including the Pharoah ant *Monomorium pharaonis*, as well as the fruit fly *Drosophila melanogaster*. We characterized 17 embryonic stages and four larval instars in worker castes. We identified diagnostic traits for each larval instar and revealed a system for determining developmental windows necessary for mechanistic studies at the larval stage. Finally, we characterized the daily morphological changes

 doi.org/10.32388/OJQCoN

observed during pupal development, an understudied phase in ant development for understanding caste differentiation. This framework will provide a foundational reference for mechanistic studies in ecological evolutionary developmental Biology (eco-evo-devo) in ants and other insects.

Travis Chen and Ab. Matteen Rafiqi contributed equally to this work.

Corresponding author: Ehab Abouheif, abouheif@zju.edu.cn

1. Introduction

The influence of development on evolution has been recognized since the dawn of evolutionary biology and has gained even greater significance with the rise of evolutionary developmental biology (evo-devo) in recent decades[1][2][3][4][5][6][7][8]. Evo-Devo focuses on organismal development to connect the black box between evolution at the level of the genotype and evolution at the level of the phenotype. Furthermore, comparing development across closely and distantly related species provides insights into how traits evolve. Comparative studies advanced significantly with the discovery of highly conserved developmental genes, which is commonly referred to as the "genetic toolkit"[9][10][11][12][13]. This discovery reinforced the idea that similar developmental mechanisms can give rise to diverse life forms, supporting the notion that small genetic alterations in the regulation of these conserved genes can drive significant evolutionary changes. However, at the morphological level, comparing features requires determining homology of embryonic features. This poses several challenges due to phenomena such as heterochrony, and lineage-specific elaborations. The discovery of the phylotypic stage, which is a stage in embryos within a phylum that show the highest level of morphological similarity, was one of the breakthroughs that made comparison across species easier[14][15][16][17]. The highly conserved phylotypic stage is symbolized by a narrow point of an ontogenetic hourglass, and an obligatory passage between two states of higher tolerance for variability[18][19][14]. These theoretical advances in development succeeded ground breaking descriptive studies in the last century included morphological maps of embryos from flies, beetles, honey bees, and ants[20][21][22][23][24][25]. More recently, detailed developmental descriptions have enabled of mechanistic studies across the insect tree of life, including: the fruit fly *Drosophila melanogaster*, the flour beetle *Tribolium castaneum,* the jewel wasp *Nasonia vitripennis,* the milkweed bug *Oncopeltus fasciatus,* the two-spotted criket *Gryllus bimaculatus,* the water strider *Gerris lacustris,* the silkworm moth *Bombyx mori,* the honeybee *Apis mellifera,* the pea aphid

Acyrthosiphon pisum, and Pharoah's ant *Monomorium pharaonis*[26][27][28][29][30][31][32][33][34][35][36][37]. Developmental tables in these insects are necessary for standardizing developmental stages between species and comparing homologous features between species. This is the first step for understanding the mechanistic basis for evolutionary change, paving the way to dissecting out the processes underlying novelty, from the highly conserved gene regulatory networks during development to morphogenesis to adult morphology. Standardized developmental staging tables play an essential role in identifying the nodes and interactions in genes regulatory networks between comparable species.

Ants belong to the family Formicidae (order Hymenoptera) with more than 20 000 described species that span all 6 habitable continents of the world[38]. Ants are also positioned at the base of insects with complete metamorphosis (Holometabola). The position of ants in relation to both insects with and without complete metamorphosis makes them highly useful for comparative developmental studies. Ants exhibit a diversity in body plans, as well as specialized, and adaptive morphologies[39][40][41][42]. Efforts to understand the developmental basis of ant body plans and their diverse morphologies have led, over the last two decades, to pioneering discoveries in the field of ecological evolutionary developmental biology (eco-evo-devo)[43][44][45][46][47][48][36][49][50][51][52][53][54]. This field focuses on how ecological, social, and symbiotic factors interact with the highly conserved genetic tool kit, and how this interaction influences development and evolution[55][56][57][58][59]. However, despite the emergence of eco-evo-devo studies in ants, comprehensive developmental tables that are necessary foundations for such studies are lacking. Historically, there were several prescient attempts to study ant development[60][61][62][30][63][64][65][48][36][25]. However, these studies had limitations: They were either not comprehensive or detailed enough to use as templates for modern mechanistic studies in ants, they did not clarify the identity of the tissues, the timing of the appearance of features, and the morphogenetic movements during development. Therefore, a comprehensive table of developmental stages has not been established so far. The developmental table of *M. pharaonis* in 2024 was the first comprehensive table of a representative ant species[36], allowing the establishment of a developmental staging system. However, recent studies investigating regulatory gene networks underlying embryonic development in ants are revealing that these networks have undergone significant alterations on relatively short timescales[48][30] (Khila and Abouheif 2010). While this makes ants an attractive model for mechanstic eco-evo-devo studies, it poses a challenge in identifying homologous developmental landmarks between species. Here, we focus on *Camponotus floridanus*[66], a species with radical alterations in embryonic development[48]. Our main aim

in this work is to establish a comprehensive developmental staging table for *C. floridanus* despite radical alterations in embryonic development.

The genus *Camponotus*[67] is a hyperdiverse ant genus with over two thousand extant species described[38][68]. A recent molecular phylogenomics study placed *Camponotus* within the monophyletic tribe Camponotini, which includes the following two other genera: *Colobopsis* and *Dinomyrmex*,[69]. The Florida Carpenter ant, *C. floridanus*, has been extensively used in the last decade as an emerging model organism for a variety of research programs including neuroscience, microbiology, pheromone, chemical communication, endosymbiotic interactions, endocrinology, genomics, epigenomics and developmental epigenetics[44][70][71][72][73][74][75][76][77][78][79][80]. *C. floridanus* can be efficiently reared in the laboratory to about 10000 individuals from single mated foundress queens, with colonies living longer than a decade[81]. Furthermore, embryonic, larval, and pupal stages can easily be collected, and experimental replicates comprising subsamples from lab colonies can be easily made[82]. Replicates can be designed to control for genetic and/or environmental variation and to evaluate functional and behavioural phenotypes. *C. floridanus* is one of the few species in the family Formicidae where laboratory experiments are relatively easy to perform. Gene function can be studied at embryonic, larval, pupal, and adult stages using RNAi, and pharmacological manipulation[74][75][48][83][78]. Furthermore, numerous other molecular techniques such as gene expression, ATACseq, and other techniques have been shown to work effectively in *C. floridanus* and other ants[44][48][49][84].

C. floridanus was one of the first complete ant genomes to be sequenced[71], along with sequenced genomes for the Argentine ant *Linepithema humile*[85], the Red harvester ant *Pogonomyrmex barbatus*[86], the Leaf cutter ant *Atta cephalotes*[87], and the Fire ant *Solenopsis invicta*[88]. The complete genome[71] as well as various methylome and histone data sets have been generated for *Camponotus*[70][79]. There are now over 250 sequenced ant genomes[89][90][91]. However, the early development of ants remains poorly studied, and a clear picture of developmental timing and standardized staging is entirely lacking. Based on the various aspects of biology being investigated in *C. floridanus*, a comprehensive developmental staging system will open enormous possibilities to address longstanding mechanistic questions, such as the effect of endosymbiotic bacteria on behaviour, caste determination, epigenetics, cell fate, and molecular basis of morphological innovations. In this paper, we characterize in detail the complete developmental stages of embryonic, larval, and pupal development covering the stages from egg to

adulthood. Despite the reported radical alterations, we were able to harmonize the staging tables between *D. melanogaster*, *M. pharaonis* and *C. floridanus*.

2. Results and Discussion

2.1. Embryonic development

We analyzed embryonic development using DIC microscopy (Figure 2) and fluorescent microscopy (Figure 3) of fixed embryos as well as movies of live embryos (Embedded Video 1). Despite the radical alterations in embryogenesis observed in *C. floridanus*[48], we were able to characterize 17 stages homologous to the stages described for *D. melanogaster*[92][27], and the ant *M. pharaonis*[36]. When the egg is laid, it is protected by two layers: the vitelline membrane, which is an acellular layer composed of proteins and the chorion, which is a hard calcified shell. To be able to image and characterize embryonic features better, we manually removed these two layers prior to imaging for all stages. Embryonic development under our laboratory conditions lasts for 12-13 days. A detailed description of the events and features of *C. floridanus* development during each of the 17 embryonic stages is as follows:

2.1.1. Embryonic Morphology

Stage 1: *0 to 5 ¾ hours after egg laying (HAEL)*. This stage is characterized by the presence of one to four nuclei, which is similar to stage 1 in *Drosophila* and *M. pharaonis,* except that the nuclei are placed towards the anterior pole of the egg (Figure 2a and 3a). Unlike these two species however, in *C. floridanus* the endosymbiotic *Blochmannia* (*Candidatus* Blochmannia)[93] are present and fluoresce intensely, appearing as a cap covering about 20% of the posterior (Figure 3a). At the boundary that separates the *Blochmannia* from the rest of the egg (at ~80 % egg length when measuring from the anterior pole as 0%), we observe a lighter-colored cytoplasm on both dorsal and ventral side of the egg (Figure 2a).

Stage 2: *5 ¾ to 16 ½ HAEL.* This stage is characterized by the presence of 8 to 256 nuclei at the anterior pole, which is similar to Stage 2 of *Drosophila* and *M. pharaonis* (Figure 3b). These nuclei are the products of the 3rd to the 8th nuclear divisions, which can be visualized as waves of cytoplasmic contractions that occur approximately every 115 minutes (Embedded Video 1; 5s - 16s). The nuclei are in a loosely organized pattern on the anterior side (Figure 3b). In the anterior region inward projections of outer plasma membrane are observed. This differs from *Drosophila* or *M. pharaonis,* where they appear at a later stage and throughout the embryo. At about 80% egg length, the embryo shows slight dents appearing laterally

as gaps in the perivitelline space (Embedded Video 1; 5s-7s), which corresponds to the position of lighter-colored cytoplasm (Figure 2b). During this stage, the embryo shortens slightly so that two more gaps are formed between the eggshell and the vitelline membrane, first at the anterior pole and then at the posterior pole (Embedded Video 1; 7s - 11s). At the same time, a part of the cytoplasm can be observed moving from the center of the egg to the posterior where the bacteria are located. The plasma membrane at the anterior ventral side of the egg begins to grow inward projections visible as a thin line parallel to the outer lining of the disc, which marks the beginning of cellularization of the germ disc (Figure 2b).

Stage 3: *16 ½ to 18 ½ HAEL*. Similar to Stage 3 of *Drosophila* and *M. pharaonis*, this stage is characterized by 512 nuclei (Figure 2c). We observe two distinct patterns in the distribution of nuclei along the length of the embryo. One region of high nuclear density in the anterior extending till approximately 25% egg length ventrally and approximately 10% egg length dorsally. This marks the formation of the presumptive germdisc in the anterior ventral region of the egg (Figure 2c). This is in contrast to *M. pharaonis* where the presumptive germdisc initiates in the posterior-ventral, and also in contrast to *Drosophila* where the germband initiates along the entire ventral region. Throughout the rest of the egg, the density of nuclei is significantly lower (Figure 3c). At the posterior pole, where *Blochmannia* reside, we can observe approximately 10 conspicuous nuclei surrounded by 'cytoplasmic halos' that are devoid of bacteria (Figure 3c). These nuclei with cytoplasmic halos are what earlier authors referred to as 'energids' in developing embryos of plants and animals[94]. We propose that these nuclei with cytoplasmic halos are homologous to the germline energids observed in *Drosophila* embryos at the same stage. However, it would require germline markers to confirm the homology.

Stage 4:*18 ½ to 24 HAEL*. Similar to *Drosophila* and *M. pharaonis*, Stage 4 in *C. floridanus* begins with the presence of 1024 nuclei and ends prior to the completion of cellularization (Figure 2d). In the region of the presumptive embryonic rudiment in the anterior-ventral of the egg, inward projections of the membranes appear deeper presumably because cellularization progresses further (Figure 2d, Figure 3d). Strikingly, a dense cytoplasmic region appears on the ventral side at 80% egg length in the shape of a crescent (blue arrowhead in Figure 3d). The nuclei with cytoplasmic halos appear more clustered at the posterior pole and are externalized (Figure 3r).

Stage 5: *24 - 35 HAEL*. Similar to the cellular blastoderm stage 5 of *Drosophila* and *M. pharaonis*, this stage is characterized by the completion of cellularization. After the membranes complete their inward projection, the germdisc appears as tightly packed columnar cells (Figure 2e,e′ and Figure 3e, s). The embryonic rudiment is now similar in appearance to the germdisc described in other insects[21], except

that it is positioned in the anterior of the egg. Using confocal microscopy, however, we can distinguish three distinct types of extraembryonic cells at this stage: (1) the serosa consists of spherical cells tightly packed anterior to the germdisc (Figure 4c-e', h-i'); (2) the amnion consists of larger and flattened cells present in the dorsal anterior region (Figure 4f-g'); and (3) large cuboidal cells, which cover the middle cylindrical part of the egg, covering an area wider at the ventral side but narrower on the dorsal side (Figure 4a-b'''). Similar cuboidal-type cells have been observed in many hymenopterans and have variably been identified as either: fat cells, trophocytes, tetratocytes, or serosa by earlier authors[95][96][97][98][48][99][25]. Our live imaging data suggests that they may eventually be consumed by the embryo at a later stage (stage 17; Embedded Video 1: 4 minutes 50 seconds onwards). We therefore propose to call these trophocytes, but this proposal requires to be further tested. The serosa and the amnion are similar in appearance to extraembryonic membranes described in other insects such as the lower flies, beetles, and wasps, although their position relative to the egg is unique in *C. floridanus*[48]. The putative trophocytes we have observed here can also be observed in other ants[36], and may be similar to the teratocytes described in endosparasitic wasps[100]. How commonly these putative trophocytes occur in other insects remains to be tested. The dense cytoplasmic region described at stage 4, which is in the shape of a crescent at 80% egg length, disappears and a large spherical cell now appears in the same location (Figure 3e). This large spherical cell has been called the germline capsule and has been shown to house the germline nuclei as well as a small population of *Blochmannia* bacteria, which are destined for vertical transmission through the gonad[48]. This germline capsule is a unique feature of the genus *Camponotus*[48]. In the posterior region the cells called bacteriocytes containing endosymbionts are now clearly visible. Each bacteriocyte contains a few zygotic nuclei and is about 40-50 micron in diameter. The cytoplasmic halos observed at the posterior pole in stage 4 (white arrowhead in Figure 3d) are now absent or hidden underneath the mass of bacteriocytes (Figure 3e).

Stage 6: *35-60 HAEL.* Similar to *Drosophila* and *M. pharaonis,* Stage 6 is characterized by gastrulation of the germdisc (Figure 2f and Figure 3f). From the ventral view (Figure 3t), a 'furrow' appears on the germdisc along its midline, oriented anterior to posterior. This marks the beginning of gastrulation, in which invagination of the presumptive mesoderm separates it from the ectoderm. This mode of gastrulation is distinct from other known hymenopterans such as *Apis mellifera* and *M. pharaonis* where a mesoderm furrow is not observed[21][36]. Live imaging shows the diameter of the germdisc becomes shorter with greater curvature (Embedded Video 1, 34s-42s). At this time, the extraembryonic serosa cells form a cap over the anterior of the egg from 0% to 25% egg length (Figure 4c-d'). The large cuboidal cells (putative

trophocytes) are observed in the same position as in stage 5. The germline capsule becomes larger, and the germline nuclei within it now appear as a spherical cluster (Figure 3f). Staining with Tubulin, a cytoskeletal marker, reveals a small slit on the lateral surface of the capsule adjacent to the cluster of germline nuclei (Figure 4a",a"'). The function of this slit remains unclear and requires further investigation. The bacteriocytes are now located more dorsally.

Stage 7: *60 – 79 HAEL*. Similar to *Drosophila* and *M. pharaonis*, this stage is characterized by initiation of germband elongation and continued expansion of extra-embryonic layers (Figure 2g, Figure 3g and Figure 4 b"-b"'; d,e) During this stage the disc-shaped embryo elongates along the AP axis on the ventral side of the yolk, forming what is typically called the germband (Embedded Video 1, 1m and 2s -1m and 15s). The posterior end of the germband is embedded underneath the large cuboidal extra-embryonic cells in the ventral (Embedded Video 1, 1m and 2s -1m and 15s). The serosa cells now start to extend to envelop the entire embryo as a lining beneath the vitelline membrane (Figure 4d-e'). The putative trophocytes appear loosely scattered underneath the serosa throughout the egg. The bacteriocytes are now more dorsally located, whereas the germline capsule is located at the posterior (Figure 2g and Figure 3g).

Stage 8: *79 – 120 HAEL*. Similar to *Drosophila* and *M. pharaonis*, this stage is characterized by germband elongation. In *C. floridanus* the germband is elongated such that the anterior and posterior ends of the germband both connect to the bacteriocytes (Figure 2h and Figure 3h). Even though segmentation has not yet begun, the germband appears undulated at this stage (white arrowheads in Figure 3h). The undulation at the anterior is slightly wider than the rest. The germband remains on the ventral side abutting a spherical yolk (Figure 3h). The amnion, which is laterally contiguous with the germband, covers the dorsal side of the yolk but not the bacteriocytes or the germline capsule (Figure 4f-f'). The serosa continues to envelop the germband, yolk, bacteriocytes, and germline capsule (underneath the vitelline membrane). The putative trophocytes are now packed around in the spaces between the serosa and the embryo (Embedded Video 1, 1m and 2s – 1m and 43s). In live imaging, the cytoplasm of the yolk sac appears very dark in colour but suddenly turns lighter (Embedded Video 1, 1m and 44s – 1m and 48s). The bacteriocytes are aggregated in the shape of a wedge on the dorsal side of the egg (Figure 2h and Figure 3h). One of the tips of the wedge is connected to the anterior end of the germband, while another tip is connected to the posterior. The germline capsule remains at the posterior pole of the egg adjacent to the germband (Figure 2h and Figure 3h).

Stage 9: *120 – 154 HAEL.* Similar to *Drosophila* and *M. pharaonis*, this stage is characterized by the completion of germband elongation such that it extends along the ventral side from the antero-dorsal to the posterior of the egg (Figure 2i, Figure 3i and Figure 5a-c). The germband is wider with denser nuclei and now forms a sharp boundary between it and the amnion (compare Figure 4f-f' with Figure 4g-g'). The germline capsule is now positioned internally with respect to the germband. The germline nuclei inside the capsule cannot be observed with DAPI staining alone at this stage. Based on germline marker staining, Rafiqi et al.,[48] have shown that the germline nuclei are located inside the germband at this stage, raising the possibility that the germline migrates across membranes from the capsule to the germband. Some of the bacteriocytes can now be observed inside the yolk sac and begin to move towards the periphery of the yolk sac (magenta arrowhead in Figure 2i and Figure 3i, and Embedded Video 1, 2m and 27s – 2m and 38s). The amnion is extended over the embryo's dorsal side, such that the bacteriocytes and germline capsule are located internally within the germband and amnion (Figure 4g-g'). The putative trophocytes are positioned around the amnion and embryo.

Stage 10: *154 – 177 HAEL.* Similar to *Drosophila* and *M. pharaonis*, this stage is characterized by the appearance of a hole in the centre of the head called the stomodeum, which will develop into the future mouth. The head is now significantly wider compared to the rest of the germband (Figure 2j, Figure 3j and Figure 5d-f). The segment boundaries are now apparent as grooves throughout the germband, which marks the beginning of morphological segmentation (Figure 5d,f). The bacteriocytes become smaller, their multiple nuclei fuse and become central, and the bacteria within are more tightly packaged (Figure 2j and Figure 3j). The bacteriocytes continue to move towards the periphery of the yolk sac (Embedded Video 1; 2 m and 38s – 2m and 45s).

Stage 11: *177 – 184 HAEL.* Similar to *Drosophila* and *M. pharaonis*, this stage is characterized by readily observable segmentation along the entire germband, in which the furrows between segments become more pronounced (Figure 2k and Figure 3k). The head develops a series of small and large lobes around its periphery, and the stomodeum becomes deeper (red arrowhead in Figure 2k and Figure 3k). The germband begins to straighten at this stage, which is typically called germband retraction (Figure 6 and Embedded Video 1; 3m and 5s – 3m and 8s). Compared to the *Drosophila* or beetle embryo where the posterior end does most of the retraction, in *C. floridanus* the retraction is bi-directional from the head as well as the tail end. Unlike in *C. floridanus, D. melanogaster* and *M. pharaonis*, initiate the process of germband retraction in Stage 12[36] (Campos-Ortega & Hartenstein). Toward the end of this stage,

tracheal pits are seen in segments T2 to A8 bilaterally (Figure 5g). The germline capsule appears to pop out dorsally (Figure 2k and Figure 3k).

Stage 12: *184 – 209 HAEL*. Similar to *Drosophila* and *M. pharaonis*, this stage is characterized by development of the head and gnathal structures. The lobes in the head become more pronounced forming the presumptive head (pro-cephalic) and mouth (gnathal) parts, including the pro-cephalic (clypeus, and a pair of hypopharyngeal lobes) and gnathal (bilateral pairs of labrum, maxilla, and mandible) parts (Figure2l, Figure3l and Figure 5j-l). Ventral to the head structures and in between the pairs of gnathal buds, the presumptive mouth is more prominent. The gnathal and hypopharyngeal lobes are oriented along the anterior, while the clypeus is oriented dorsally (Figure 5k,l). A pair of large lobes are formed dorsal to the hypopharyngeal buds and on the sides of the clypeus, whose position is homologous to the optic lobe in other insects (Figure 5k,l). Germband retraction and straightening of the germband, proceed further (Figure 6). The germline capsule is now not as prominently popped out as in the previous stage (Figure 2l and Figure 3l).

Stage 13: *209 – 220 HAEL*. Similar to *Drosophila* and *M. pharaonis*, this marks the end of germband retraction and the beginning of dorsal closure, which can be seen as a reduction of the distance between the edges of the epidermis (Figure 2m and Figure 3m). The procephalic buds are observed more anteriorly and the gnathal buds are more pronounced and slightly ventral in orientation (Figure 5n,o). In the posterior, proctodeal invagination becomes observable (Figure 2m and Figure 3m). The germline capsule, which was in a dorsal position is now seen in the ventral and posterior position just adjacent to the germband (Figure 2m and Figure 3m). Live imaging shows that the germline capsule moves as if a balloon passes through a narrow constriction (Embedded Video 1; 3m and 32s – 3m and 41s).

Stage 14: *220 – 232 HAEL*. Similar to *M. pharaonis*, in this stage the procephalic and gnathal buds are now arranged into a circle in the anterior giving rise to the lining of the future larval mouth (Figure 2n and Figure 3n). For higher flies such as *D. melanogaster*, this stage is characterized by the process of head involution giving rise to headless larvae. This process is specific to that suborder of true flies but is absent in other insects including ants. The segment boundaries continue to become more pronounced, and the proctodeal invagination is clearly visible (Figure 3n). The process of dorsal closure proceeds similar to *M. pharaonis* as closing of the gap between the edges of the epidermis, but unlike *D. melanogaster*, none of the segments are yet closed dorsally.

Stage 15: *232 – 252 HAEL*. Similar to *D. melanogaster* and *M. pharaonis*, this stage is characterized by the completion of dorsal closure. Dorsal closure is accomplished when the lateral epidermis joins at the

dorsal side of the embryo starting from the anterior and posterior ends and closing towards the mid region. At the same time, the gnathal buds appear shifted slightly ventral giving a more constricted spherical pattern. The optic lobes are now internal to the outer epidermis of the embryo (Figure 2o and Figure 3o).

Stage 16: *252 – 285 HAEL*. Similar to *M. pharaonis*, during this stage the larval mouth is placed further ventrally and becomes further constricted (Figure 2p and Figure 3p). The embryo around the abdominal segments takes the form of a barrel, while the body around the thoracic segments is narrower and longer. The midgut and germline capsule are reduced in size compared to earlier stages (blue arrowheads in Figure 2p and Figure 3p).

Stage 17: *12th day AEL*. Similar to *D. melanogaster* and *M. pharaonis* this stage marks the end of embryogenesis. The pre-larva is fully formed inside the eggshell consisting of a layer of loosely attached putative trophocytes, the serosa, and the vitelline membrane. The germline capsule can be observed in the posterior of the abdomen as a highly reduced sphere, which is not observable towards the end of this stage (Figure 2q and Figure 3q). The pre-larva begins to wiggle inside the eggshell and consumes the putative trophocytes (Embedded Video 1; 4m and 52s – 5m and 05s). The gut contents appear to be actively moving (Embedded Video 1;5m and 8s – 5m and 33s). The body around the thoracic region becomes even narrower and the pre-larva further elongates, curving its head ventrally. The larva then hatches from the eggshell.

2.1.2. Duration

Embryonic development takes approximately 13 days from the time an egg is laid by the Queen. We observed some variation in duration of embryonic development in embryos that were reared without workers; these embryos develop relatively faster (data not shown). The duration of specific stages taken as percentage of total time of duration (13 days being 100%) showed an overall scaling of the durations with some key differences. Durations of stages 1, 6, 7, 8, 9, 10, and 16 were shorter compared to the corresponding stages in *Drosophila*. Whereas, stage 2, 3, 4, 5, 11, 12, 13, 14, 15, and 17 were significantly longer than the corresponding stages in *Drosophila*. In comparison to *M. pharaonis* stages 1-5 and 11-13 are proportionately shorter while as stages 6-9 and 14-17 are proportionately longer in *C. floridanus*. Overall, these data show that development is slower between the stages 8 and 10 in *C. floridanus* compared to *Drosophila* and is conspicuously faster in stage 11 compared to *Monomorium*. This is in addition to the fact

that development is 13 times slower in *C. floridanus* than in *Drosophila* in absolute time and is slightly slower than *M. pharaonis* by two days (Figure 7).

The duration of embryonic development has been shown to be affected by the presence of workers[30]. In *C. floridanus*, we also noted that embryos that were allowed to develop in the absence of workers on water agar plates developed much faster than the embryos that were accompanied by the workers (unpublished observations). This phenomenon may be attributed to the founding of colonies where the initial eggs are accelerated in development to establish a colony as fast as possible to supply the colony with foragers[101].

In summary, despite the radical alterations in embryogenesis described by[48], we were able to assign 17 embryonic stages of the carpenter ant *C. floridanus* that are homologous to those of *D. melanogaster*[92] [27] and the ant *M. pharaonis*[36]. Furthermore, the proportionate duration of stages fairly corresponds with those described earlier for other insects with a few minor exceptions in morphology described above (Figure 8).

2.2. Larval development

The number of larval instars in *C. floridanus* has previously been a matter of debate, being described as having anywhere between 2 to 5 larval instars[102][77][103][104]. The number of larval instars reported more broadly within the ant tribe *Camponotini* (the tribe to which *C. floridanus* belongs) also varies between 3 to 5[105][106][107][108][109][110][111]. For example, 4 instars were reported for *Camponotus textor*[110], 3 were reported for *Camponotus vittatus*[109], and 4 were reported for *Camponotus japonicus*[108]. The variation reported in these cases is likely due to the different methods used to determine the number of larval instars, which range from a purely qualitative assessment to the more rigorous method of measuring head capsule width against frequency of the larvae[112]. In *C. floridanus*, Alvarado et al. [44] previously found 4 larval instars by plotting head capsule width and larval length. Here we sought to confirm the number of larval instars in *C. floridanus* by measuring mandibular length[112]. Although difficult to measure, mandibular length also provides a rigorous measure of the number of larval instars because the mandibles and head capsule are sclerotized (hard) parts of the larval body. Therefore, these hard parts only grow between instars when the surrounding cuticle is shed but not within instars. Using mandibular length, we found that the distribution of sample number of larvae collected from a *C. floridanus* colony shows four distinct modal distributions confirming the existence of four larval instars (Figure 9).

In *C. floridanus*, we observed high variability between individual larvae in the duration of larval development within each instar (see Figure 13a). 1st instar larvae were observed 13 days after egg laying and were observed as 1st instar between 6 and 13 days after hatching. Specifically, about 75% of the 1st instar larvae were observed for 6 days, while the remaining continued to be observed gradually decreasing in number up until the 13th day after hatching. 2nd instar larvae were first observed on the 6th day after hatching and were observed for at least 4 days after their molting. 3rd instar larvae were first observed on the 10th day after hatching and continued to be observed for a minimum of 4 days. The 4th instar larvae were first observed on the 14th day after hatching and continued for a minimum of 5 days after that before they started spinning a cocoon and transitioned into the pupal stage. In total, the minimum duration of larval development was 19 days. After 19 days of larval development, 2, 3, and 4th instar larvae remained observable in our experimental replicates, gradually decreasing in numbers. The duration of all larval instars has also been reported to be highly varied between individual larvae in *C. japonicus*[108].

Alvarado et al.[44] have suggested that larvae are determined as minor or major worker-destined larvae during the last (4th) instar as that is the instar where the majority of larval growth is generated. During the last instar, larvae undergo rapid growth after they are determined as minor or major workers. Developmental time in *C. floridanus* is correlated to final larval size, such that the smaller minor workers develop for a shorter period, than the larger major workers. Because *C. floridanus* minor and major worker larvae vary continuously in size, the duration of larval instars is highly varied between individual larvae. Once larvae reach the terminal stage as reflected by their gut color, just before pupation, they attain their final larval size (see Figure 12 and detailed description below under "4th instar larvae"). At this point, the relative size of larvae in the colony reflects their relative size as adults in the colony (Hanna et al. 2023). These and the following descriptions provide a road map for identifying developmental windows or critical periods during which worker subcaste determination takes place, which is key for enabling mechanistic studies of larval caste determination in this species. Alvarado et al.[44], for example, explored these developmental windows to investigate the role of epigenetic modifications in quantitative worker sizing and caste-specific development, and more recently, MacMillan et al.,[113] explored them to show that minor worker and soldier castes in *C. floridanus* are determined by a developmental switch mediated by JH signaling.

2.2.1. Larval morphology

1st instar larvae (Figure 10 a, e, h, Figure 11 a-c, a') – The 1st instar larvae have mandibular lengths of 70-77 μm (Figure 9), and Alvarado et al.,[44] describes the head capsule width of 300 μm to 340 μm, and a length of 800 μm to 1100 μm. They are slightly off-white and opaque; a very slight light brown coloring can be observed in the abdomen if the larvae have been fed. From the head capsule to the posterior the larvae consist of 3 thoracic segments (T1-3), 10 abdominal segments (A1-10), and a subterminal anus. From a ventral view the body of the 1st instar larvae is widest at A5 and tapers towards both the anterior and posterior, with a shallower taper towards the anterior (Figure 10 e). A pair of eye spots are seen anteriorly above the mouth (Figure 11a). From a lateral view, the mouth is seen ventrally oriented, the eye spots are anterior. The T1-T3 segment boundaries are offset between their ventral and dorsal sides and together are wider dorsally and narrower ventrally. The gula is seen anterior to the T1 on the ventral side (Figure 10h). Large spiracles can be observed as holes on the lateral sides of the larvae in segments T2, T3, as well as A1-A8 (Figure 10h). The 1st instar larvae lack hairs on the posterior end, yet have cuticular hairs on the head capsule and two pairs on the sides of the gula (Figure 11 a,c), consisting mostly of short (30 μm - 45 μm) unbranched smooth slightly curved, or uncinate forms[114]. A pair of antennae can be observed on the head capsule along with a pair of very pronounced tentorial pits (Figure 11a'). Unbranched smooth hairs can be found on the clypeus and above the labrum. Unbranched uncinate hairs can be seen on the gena (side of the frons) and ventral side of the labrum. Multiple setaceous and basiconic sensillae can be observed on the labrum. Small pinhead-like protuberances of the galea and palps can be observed on the maxilla and the labium. The mandibles are camponotoid subtriangular and smooth. The head is proportionately larger than the body in the first instar compared to the later instars.

2nd instar larvae (Figure 10b, f, i and Figure 11 d-g) – The 2nd instar larvae have mandibular lengths of 100-120 μm (Figure 9), and Alvarado et al.,[44] describes the head capsule width of 370um to 410um, and a length of 1200um to 1450um. They are slightly off-white and opaque, and the gut has a light yellow-brown opaque pigmentation from ingested contents. From a ventral view (Figure 10f) the body of the 2nd instar larvae has a more uniform body width compared to 1st instar larvae, with very little tapering towards the anterior and significant tapering towards the posterior only starting at segment A8. As with the 1st instar larvae the gula tapers from the ventral towards the dorsal. Also like the 1st instar larvae, spiracles can be observed on the lateral side of the larvae on segments T2, T3, and A1-A8 (Figure 10i). The 2nd instar larvae have cuticular hair on the head capsule, as well as T1-T3, A3, A9, A10 segments (Figure 11

d), and around the anus (Figure 11e). The cuticular hairs on the 2nd instar larvae are unbranched smooth and predominantly uncinate with a few straight ones found on the head capsule. A pair of antennae with 3 sensillae each can be observed on the head capsule, along with a pair of tentorial pits that are less pronounced compared to the 1st instar (Figure 11d, g). Unbranched smooth uncinate hairs can be found on the head capsule. Multiple sensilla can be observed on the galena and palps on the maxillae, and on the labium (Figure 11d). The cuticular hairs on the thorax, abdomen, and anus are generally longer (75 µm – 85 µm) than the hairs on the head capsule (55 µm – 60 µm). A pair of short uncinate hairs can be found on each side of the ventral-lateral of the gula. Cuticular hairs on T1 and T2 segments are predominantly found on the dorsal and dorsal lateral of the segment (Figure 10i). A single cuticular hair is seen on the lateral surface of T3 and at the central point on the ventral surface of the A3 and A7 segments (Figure 10i). A pair of cuticular hairs can be seen equally spaced from the center on the ventral surface of the A8 segment (Figure10f). There are several hairs on A9 and a couple on the A10 segment around the anus (Figure 10f, 11e).

3rd instar larvae (Figure 10c, g, j and Figure 11 h-l) – The 3rd instar larvae have mandibular lengths of 144-160 µm (Figure 9), and Alvarado et al.,[44] describes the head capsule width of 450 µm to 530 µm, and a length of 1600 µm to 2700 µm. They are slightly off-white and opaque; the gut has a light yellow-brown opaque pigmentation from ingested contents. From a ventral view (Figure 10c, g) the body of the 3rd instar larvae has wider central abdominal segments, tapers slightly from segment T3 towards the anterior, and tapers more dramatically from segments A7 towards the posterior. The proportionate growth of the larval thorax and abdomen is greater than that of the head (compare Figures 10a, 10b, with 10c). Spiracles, which are present in T2, T3 and A1-A8 are mostly covered by the cuticular hairs but may be observable in a few of the segments (Figure 10j). The cuticular hairs on the head capsule are sparser compared to the larval body and lack longer hairs, while all types of hairs can be found on the head capsule, it is overwhelmingly comprised of unbranched smooth straight/slightly curved hairs (Figure 11h). A pair of antennae with 3 sensillae can be observed on the head capsule (Figure 10g, 11h). The pair of tentorial pits are less pronounced compared to the 2nd instar, whereas the galena and maxillary palps are more pronounced compared to the 2nd instar (Figure 11h, compared to 11d). A mixture of cuticular hair uniformly covers the larvae, which comprise of predominantly short cuticular hairs (60 µm) with a sparse distribution of long hairs. More specifically, the types of hair found on the 3rd instar larvae are: unbranched smooth uncinate, unbranched smooth straight/slightly curved, branched bifid smooth deeply bifid, and branched multifid and smooth branching dichotomously (Figure 11h-11l).

4th instar larvae (Figure 10d, k, and Figure 11m-q) – The 4th instar larvae have mandibular lengths of 194-212 μm (Figure 9a), and Alvarado et al.,[44] describes the head capsule width of 590 μm to 630 μm, and a length of 3000 μm to 7800 μm. Depending on the size and how close to pupation the larva is, the colour and opacity ranges from slightly off white to whiter, and from slightly translucent to opaque. This difference is consistent with the size of fat bodies observed in the larvae, when they are dissected. They are bigger in soldier larvae that are whiter and more opaque compared to minor worker larvae. From a ventral view (Figure 10d) the body of the 4th instar larvae have uniform central abdominal segments, which tapers slightly from segment A1 towards the anterior, and tapers more dramatically from segments A8 towards the posterior. The proportions of the head capsule compared to the other instars is much smaller. The spiracles are covered by cuticular hairs and cannot be observed. The only types of cuticular hair on the head capsule are unbranched smooth straight or slightly curved, that measure approximately 85 μm to 100 μm long. A more prominently visible pair of antennae with 3 sensillae can be observed on the head capsule, along with a pair of tentorial pits that are shaped like slits (Figure 11m). The galena and maxillary palps are more pronounced compared to the 3rd instar larvae. The central tip of the labium contains the sericteries (the silk gland), where the silk for spinning cocoons is produced and released (Figure 11m). A mixture of cuticular hairs uniformly cover the larval body, compared to the 3rd instar. The cuticular hairs on the body are denser and uniform in size (70 μm to 90 μm). The types of hairs found on the 4th instar larvae are: unbranched denticulate found throughout the length, as well as unbranched smooth uncinate, branched bifid smooth, deeply bifid, branched multifid, and smooth branching dichotomously (Figure 11n-q).

During the 4th larval instar, whether the larvae is minor-worker or soldier-destined, the colour of the larval gut changes progressively as larvae develop from yellowish (Figure 12a, a' and b, b') to light brown (Figure 12c, c' and d, d') to brown (Figure 12e, e' and f, f'), indicating that the larvae are still developing. When the larval gut color becomes dark brown (Figure 12g, g' and h, h') the larva ceases growth and is at the terminal stage. The size of the larvae at this stage is correlated to the relative size of adults (Hanna et al. 2023). Finally, when the larval gut color turns black (Figure 12 i, i' and j, j'), this marks the onset of pupation. Larval gut color is critical for determining the precise timing of experimental manipulations, such as RNAi injections or other experimental treatments, which must be administered while larvae are early enough in their development (Figure a, a'- c, c') to elicit phenotypic effects.

Finally, we tracked the timing of development of individual larvae through to the adult stage, tracking the size at which the larvae reached the terminal stage, the number of days it took to eclose as a pupa, and

final head and body size of adults. We show that larval developmental time is correlated to both the size of terminal larvae and whether it will develop into a small-headed minor worker or large-headed soldier. Larvae that are smaller at the terminal stage (between 5-6mm), develop for a shorter period before they metamorphose into small-headed adult minor workers (Figure 13 b, c). In contrast, larvae that are larger at the terminal stage (6mm and above), develop for a relatively longer period, and metamorphose into large-headed adult soldiers (Figure 13b, c). Our findings therefore suggest that there is a sharp threshold at approximately 6mm in larval size, such that larvae that are less than 6mm (minor worker-destined larvae, blue dots) versus those that are more than 6mm (soldier-destined larvae, red dots) produce a discontinuous break in head size between adult minor workers and adult soldiers (Figure 13b). In contrast, body size is continuous, such that terminal stage larvae that are continuously larger at the terminal stage are continuously larger as adults (Figure 13c). Altogether, our findings are consistent with those of previous studies showing developmental time and thresholds are important factors in regulating head and body size between worker subcastes (minor workers and soldiers)[115][116][117].

2.3. Pupal Development

Pupal development ranged from 21 to 27 days for workers (Figure 14-16), this variation in developmental time correlates with the terminal larval length (data not shown). The development ranged from 21 to 23 days for minor workers and from 24 to 27 days for major workers. Pupal morphology was analyzed from images depicting twenty average sized minor worker destined pupae (Figure 14-16). During the transition to the pupal stages, the larva moves its head and body, produces silk from its sericteries, and spins a cocoon around itself. The cocoon is a uniform and thin membrane created by repeatedly layering strands of silk in a disordered mesh. In the wild and under optimal lab conditions the larva produces a cocoon. However, under conditions of stress we observe larvae undergoing pupation without a cocoon. Although, *C. floridanus* larvae are able to undergo successful pupation into an adult ant without a cocoon the survival of these pupae is compromised due to multiple factors including exposure to infections. This phase of pupal development could be considered homologous to the wandering phase in *Drosophila* by the fact that it is non-feeding but mobile unlike the pupa[118].

The first phase of pupation lasts from day 0 till day 3. The youngest cocoons were white while the older ones were of a tan colour. The prepupal mouth was initially positioned ventrally similar to the 4^{th} instar larvae, while dark gut contents were observed at the mid-section along their length (Figure 14a, 15a, 16a). The mouth and body were distended by day 2 so that the mouth was more anterior (Figure 14b, 15b, 16b).

In 2 to 3 days old pupae, the dark contents of the gut were observed more posteriorly, and the body was slightly more stretched along its length (Figure 14c-d, 15c-d, 16c-d).

The second phase of pupation starts on day 4 and lasts till day 6 and is the last phase during which the larval cuticle remains intact (Figure 14d-f, 15d-f, 16d-f). It is characterized by the presence of expelled gut contents as meconium attached to the inside of the cocoon near the anus, where it remains until eclosion. The ventral of the thoracic region appears translucent, which expands and eventually shrinks to shape upon adult features, of which leg shapes are discernible (Figure 14f, 15f, 16f).

The third phase starts on day 6 and lasts till day 17 and is the period beginning with the shedding of the larval cuticle (Figure 14 g-q, 15 g-q, 16 g-q). The pupae had a fully formed exoskeleton with antennae, legs, head and thorax, along with varying levels of petiole and abdomen formation, from less to more defined. The abdomen was smoother, and the petiole initially appeared as a continuation of the curvature of the abdomen (Figure 15g) but later was more distinct (Figure 15 h-q). Between days 6 to 7 light-brown translucent pigmentation was observed at the posterior dorsal part of the eyes (Figure 14g, 15g, 16g). Older pupae showed progressively greater area of the eyes pigmented. By days 9 to 10, the eyes were pigmented throughout, but pigmentation was reddish-brown and darker at the posterior dorsal of the eye (Figure 14j, 15j, 16j). The eyes of even older pupae appeared more pigmented so that at day16-17 they were dark black (Figure14q, 15q, 16q).

The fourth and final phase of pupation starts on day 17 and lasts till day 20 and is characterized by pigmentation of the body cuticle (Figure 14r-t, 15 r-t, 16 r-t). By day 16 to 17 the body has a light yellow-brown color earliest at the thorax, around the mandibles, at the anterior part of the legs, at the joints, at the petiole and abdomen, although more pronounced in the petiole and abdomen (Figure14r, 15r, 16r). Between days 17 to 19 (Figure 14 s, 15s, 16 s), the pigmentation of the exoskeleton was seen in the legs, antennae, head and thorax. Between days 19-20, the abdomen and petiole were brown, and the rest of the body was orange (Figure 14t, 15t, 16t). These progressively darker pupae were observed till the end of pupal development at day 21- 22. The darkening of the cuticle is also observed in the callows (young adults) in the days following eclosion. Finally, we also observed (unpublished observations) that pupal eclosion time might be conversely affected by the presence of minor workers. Minor workers open the cocoon and ‘wake’ the callows up; they thus likely hasten the pupal stage duration. Therefore, future work should investigate how and why pupal development accelerates or decelerates in the presence or absence of workers.

Individuals during pupal development were overall inactive with a few exceptions. When imaging pupae that had been dissected out of their cocoons, some pupae showed regular contractions with interceding pauses in their abdomen. This activity was observed from day 5 to 9 after cocoon formation, although most activity was noted at day 8-9 (6 out of 12 occurrences).

The changes accompanying pupation are most dramatic between days 5, 6 and 7 when the appendages are extended outwards, which makes the pupa resemble the adult most closely[119]. The description of pupal development in reproductive castes (males and queens) was not undertaken here due to the lack of an established method for induction of reproductive castes in an experimental setting for *C. floridanus*. Although we have observed the development of males in orphaned colonies under specific conditions, the lack of availability of abundant material has not allowed us to do these experiments. It should, however, be possible in the future to describe pupal development of reproductive castes, although significant differences in timing are not expected based on observations in *M. pharaonis*[36]. The pupal stage is used in many systems across insects to effectively knockdown genes using parental RNAi for testing maternal effect genes[120][121][122]. The critical changes occurring during pupal period could be used as landmarks towards understanding the molecular developmental mechanisms underlying morphogenesis and caste differentiation. This staging of pupal development in *C. floridanus* will enable comparisons across ants and other insects, paving the way for a mechanistic understanding of the evolution of morphogenesis in insects.

3. Conclusion

Despite the challenges in working with emerging models that show radical alterations in embryonic development, we have successfully described 17 embryonic stages, 4 larval instars, and the daily progression of the pupae of the Florida carpenter ant *C. floridanus.* We aim for this developmental staging table to provide a guide for mechanistic studies in the field of eco-evo-devo of ants (Figure 17). We hope this developmental staging table, along with that of the Pharoah's ant *M. pharoanis*, will serve as blueprints to establish developmental staging tables for each of the approximately 365 ant genera. Only then will it be possible to gain a complete understanding of caste determination and differentiation and morphogenesis through mechanistic studies. The interest in understanding developmental processes at the organismal level is ever growing, and it is abundantly clear that any single level of exploration is not sufficient to provide complete answers to questions of interest for biology in particular and science in general.

4. Materials and Methods

4.1. Ant collection and maintenance

Mated queens of *C. floridanus* were collected in Tallahassee, Florida, USA in 2007. Mature colonies originating from a single queen were kept in sealed plastic boxes with a metal mesh-covered hole in the lid. The inside walls of the boxes were coated with a fluoropolymer resin (BioQuip – Insect-a-Slip Insect Barrier – Fluon®) to prevent the ants from climbing on the walls. The boxes contained multiple disposable glass tubes half filled with water and plugged with cotton wool, and a single tube filled with 0.7M sucrose, also plugged with cotton. The tubes were held in place with modelling clay and a red translucent cellophane film used to cover the water tubes to simulate darkness. The colonies were fed Bhatkar-Whitcomb diet[123] supplemented with fresh mealworms. The colonies were kept at 25°C, 65% humidity, and 12h day: night cycle unless indicated otherwise. Embryo collection experiments were done with colonies that have been maintained for approximately 7 years.

4.2. Embryo Collection

Mated *C. floridanus* queens from three different colonies were isolated separately in small Fluon®-coated plastic boxes each with 25 workers. Two small test tubes half filled with water, and or filled with 0.7M sucrose in water, both plugged with cotton. These colonies were not in the process of producing reproductives (males or queens). Embryos were collected from each queen daily for 14 days and kept in separate boxes. Workers accompanied the embryos in excess to ensure optimal care. Workers were taken from the box harbouring the queen and the box containing the original colony to supplement the experimental replicates. Workers were also taken from the original colony and supplemented to the box containing the queen when needed. Replicates were fed as often as the parent colony.

4.3. Embryo fixation

Embryos were placed in a 1.5ml Eppendorf tube with 100 μl PBS-triton (1.86mM NaH_2PO_4; 8.41mM Na_2HPO_4; 1.75M NaCl; 0.03% Triton-X-100, pH 7.4). The tubes containing the samples were cooled on ice for 10 minutes, then placed in boiling hot water bath for exactly 30 seconds and subsequently placed on ice. 1mL of ice-cold PBS (1.86mM NaH_2PO_4; 8.41mM Na_2HPO_4; 1.75M NaCl; pH 7.4) was immediately added and samples were incubated on ice for 5 minutes. Embryos were then transferred to a heptane/formaldehyde solution in a 1.5ml Eppendorf tube consisting of 50 μl formaldehyde, 450 μl PBS-

tween (1.86 mM NaH_2PO_4; 8.41 mM Na_2HPO_4; 1.75 M NaCl; 0.05% Tween-20), and 500 μl heptane. The tubes were incubated on an orbital shaker for 20 minutes. The lower phase (PBS-tween/formaldehyde) was removed, and 500 μl freezer-cold methanol was added and the tube inverted several times to mix; subsequently the solution was removed followed by two additional washes of 1ml cold methanol with 5 minutes of rotation on the orbital rotator between each wash. The embryos were stored in methanol at -30°C.

4.4. Embryo poking and dissection

Tungsten dissecting needles were made as previously described[124]. Tungsten wire (.005in or .127mm) was placed in a holder and sharpened by repeatedly dipping for electrolysis at 5-12V and 1M NaOH as electrolyte. The vitelline membrane of the embryo was gently poked with the needle to permit efficient penetration of stain when needed. A select number of embryos had the entire vitelline membrane removed using tungsten dissecting needle and forceps. Embryos were dissected in a 50:50 PBS:Glycerol solution.

4.5. DAPI staining

Fixed and poked embryos were incubated in a 1:2000 DAPI:PBS solution and placed on the orbital rotator for 2h in a cold dark room and subsequently normalized in 50:50 PBS:Glycerol solution for 1h (1:2000 DAPI:PBS and Glycerol). Alternatively, the embryos were incubated in a 50:50 DAPI/PBS:Glycerol solution for 24h to stain.

4.6. Immunostaining

Embryos collected from colonies were first fixed with 5% formaldehyde solution in phosphate-buffered saline with 0.1% Tween 20 (PBST). The vitellin membrane was gently peeled off using a tungsten needle. Peeled embryos were then washed several times in PBST. The samples were blocked for 1 h in blocking solution (5% normal goat serum in PBST) at room temperature. Embryos were incubated overnight at 4 °C with the primary antibody against α-Tubulin tubulin (DSHB AB_2315513)[125] diluted 1:250 in blocking solution. Following primary incubation, embryos were washed 3 times 10 mins each in PBST and then incubated with an Alexa Fluor–conjugated secondary antibody A488 (1:500 in blocking solution) for 2 h at room temperature in the dark. After secondary incubation, embryos were washed 3 times 10 mins each in PBST and gradually transferred into increasing concentrations of glycerol (25%, 50%, and 75%) for

mounting. Embryos were carefully removed by pipetting with a cut tip and placed on a microscope slide for further analysis under fluorescence microscope.

4.7. Embryo imaging

The embryos in 50:50 DAPI/PBS:Glycerol solution were placed on a glass slide. Spacers made of modelling clay, small coverslips or scotch tape were placed on the glass slide to prevent crushing of the embryos before adding a coverslip on the embryos. Images of the embryos were taken with Zeiss ImagerZ1 microscope using preconfigured DAPI and DIC settings. Z-stacks and extended focus were done using Zeiss Axiovision software (Carl Zeiss Canada Ltd, Toronto, Ontario, Canada). Confocal images were taken using a Leica SP8 inverted microscope.

Images were cropped and processed using Adobe Photoshop CS5 (Adobe Systems Inc., San Jose, California, USA). Brightness, contrast, levels, and sharpness adjustments were made to the image as a whole. To ensure that fluorescent signals were not a result of auto-fluorescence, embryos that were of the same age but had not been stained with DAPI were imaged alongside stained embryos. To the same end, embryos were imaged using other fluorescent ranges such as GFP and Cy5 and no specific signal was observed.

4.8. Time-lapse imaging of embryonic development

Queens were isolated in smaller setups along with 5-10 workers and about 10 larvae. Prior to embryo collection, heptane glue (heptane infused overnight with double side sticky tape) was applied to the bottom of wells of a 96 well cell culture plate and allowed to dry. Freshly laid embryos were collected and were placed and oriented on the glue coated wells of the plate. Embryos were covered with a drop of halocarbon oil 700 (Sigma, H8898). Time-lapse recordings were performed using cell imaging multi-mode plate reader Cytation™ 5 (Biotek, Winooski, VT). Z-series consisting of 2 positions surface and center of embryo were captured for each well at 5-minute intervals beginning at the collection time. Imaging was continued for 14 days. A 4 x phase-contrast objective was used. Higher than optimal exposure was used in order to visualize internal structures. Gen5™ software (Biotek, Winooski, VT) was used to choose individual focal planes for each time point. The images were aligned and then converted into movies using Image-J software[126].

4.9. Larval instar duration

A mated queen was isolated with 150 workers and soldiers in a setup as described above. The setup was kept at 28°C, 65% relative humidity, and a 12h day:night cycle. After 24 hours embryo deposition, the queen was removed from the experimental replicate and returned to the parent colony so that there are no more freshly laid embryos. Upon the first observation of 1st instar larvae, all unhatched embryos were removed from the experimental replicate and the queen was placed into the experimental replicate for the rest of larval development to avoid any confounding effects due to long term absence of the queen. The larvae were monitored daily for transitions between instars. The newly laid eggs and embryos were periodically removed so that there were no new larvae entering the replicate after the beginning of observation.

4.10. SEM of Larval Instars

Two larvae from each of the instars were collected and oriented ventrally and laterally. The larvae were mounted on a carbon tab, which was then placed on a specimen mount. The SEM pictures were taken with the Hitachi TM3030 tabletop microscope. Images were cropped and processed using Adobe Photoshop CS5 (Adobe Systems Inc., San Jose, California, USA). Brightness, contrast, levels, and sharpness adjustments were made to the image as a whole.

4.11. Larval gut colour

To characterize gut colour, larvae of similar length representing different stages on the gut pigmentation scale were sampled from the same laboratory colony. Each larva was imaged in both lateral and dorsal views under bright-field illumination using Zeiss Axiovision software (Carl Zeiss Canada Ltd., Toronto, Ontario, Canada).

To confirm that gut pigmentation correlated with developmental progression, individual larvae were fixed and stained with DAPI to assess leg disc development as a proxy for overall growth status. Imaging was performed using a Zeiss Imager Z1 microscope with preconfigured DAPI settings. Z-stacks and extended focus images were generated using Zeiss Axiovision software.

4.12. Culturing Pupae

Late 4th instar larvae from a single source colony were isolated with minor workers (2:1 minor worker to larva ratio), in a plastic box coated with Fluon®, until cocoon formation. The box contained glass tubes

half filled with water and plugged with cotton wool, and a single tube filled with 0.7M sucrose, also plugged with cotton. The tubes were held in place with modelling clay and covered with a red translucent cellophane film.

Late 4^{th} instar larvae were collected and were monitored for initiation of pupation. Pupae were isolated with 5 minor workers in 18x150mm tubes containing half-way filled water restrained with cotton. Plastic drinking straws were cut in inch-long sections and filled with Bhatkar-Whitcomb diet. The straws were then wrapped in cotton and that was used to seal the tubes' opening. Fresh food was replaced every 4 days. Dead workers were replaced with workers from the colony. These setups were kept horizontally in an incubator at 25 ˚C, at a relative humidity of 60% and 12h day:night cycle. Cocoons were removed manually before imaging. Prepupae with a body size of around 5650 μm at their larval terminal stage, sclerotized pupae with a scape length of around 2050 μm, whose pupal stage lasted 22 days was taken as the standard. The time points given in this paper only apply for individuals of these specific sizes.

4.13. Imaging Pupae

The pupae were dissected out of their cocoon, placed in a clean Petri dish, over a black sheet of paper and imaged using AxioVision SE64 (Carl Zeiss Canada Ltd, Toronto, Ontario, Canada) from different angles: ventral, lateral and dorsal. Images were cropped and had their levels adjusted as a whole using Adobe Photoshop CS5 (Adobe Systems Inc., San Jose, California, USA).

Figures

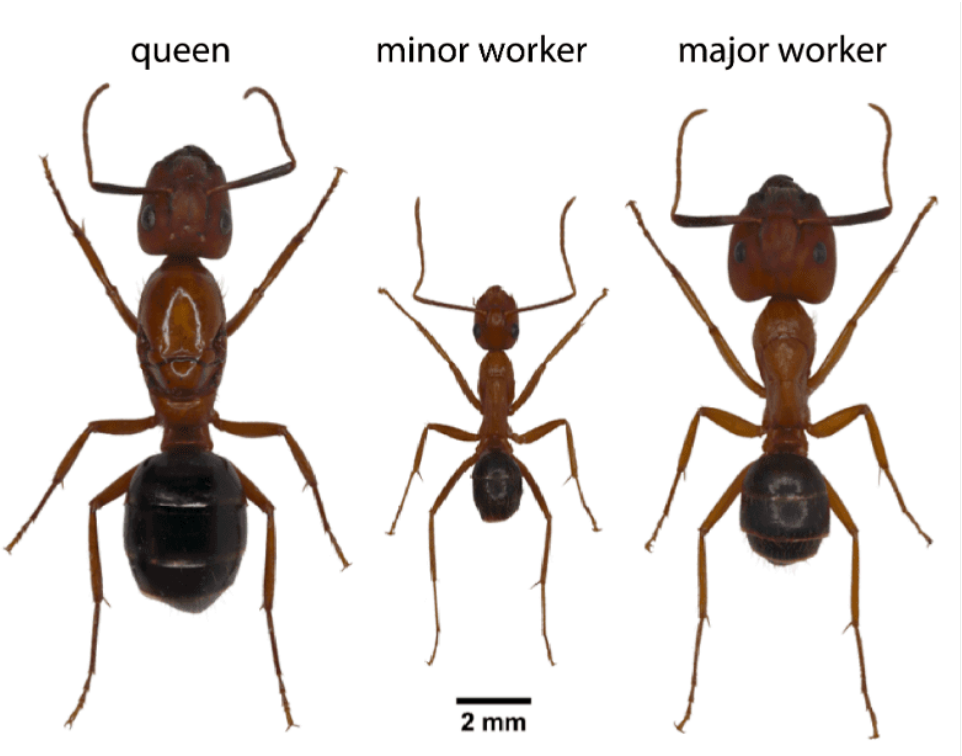

Figure 1. Adult of queen, and representative minor worker and major worker (soldier) of the Florida carpenter ant *Camponotus floridanus*. Photos by Erik Plante and Dominic Ouellette.

doi.org/10.32388/OJQCoN

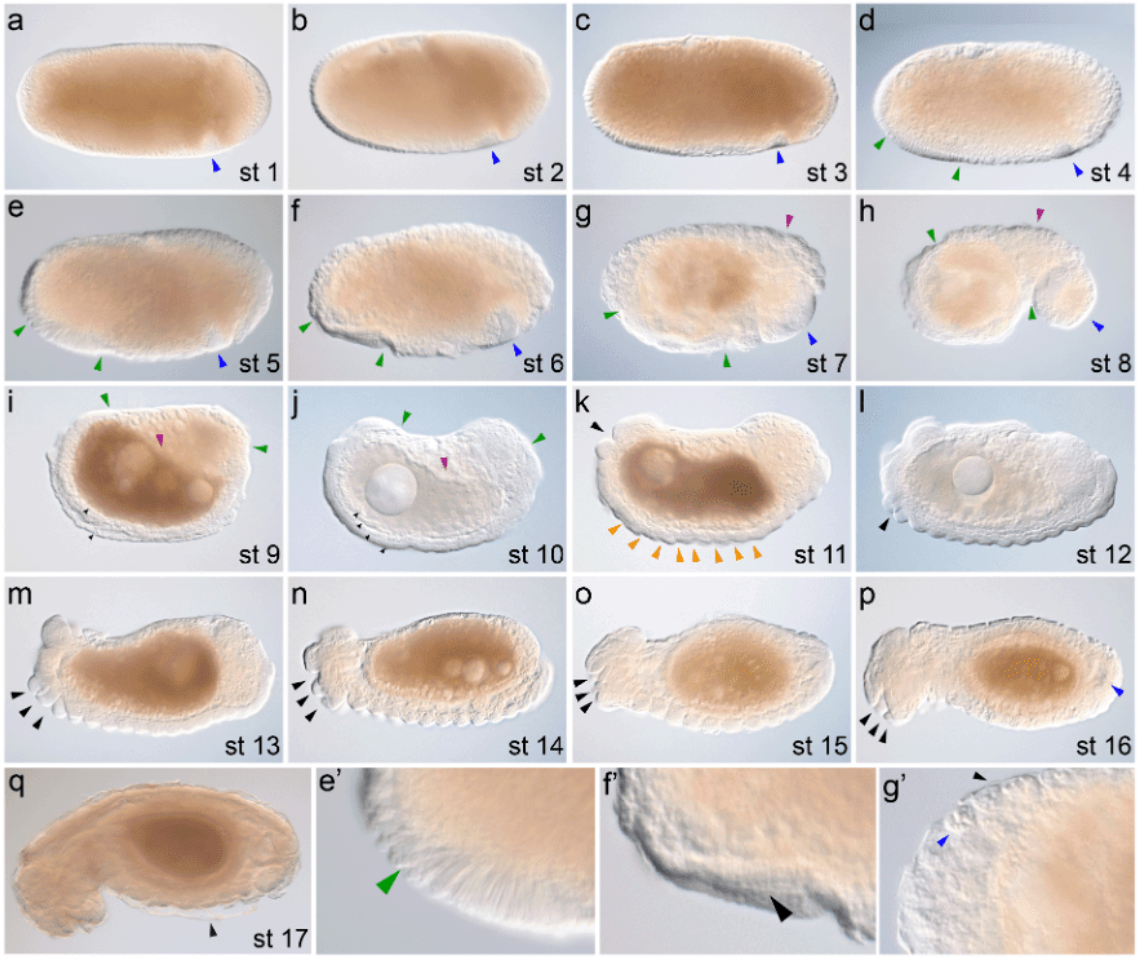

Figure 2. Differential interference contrast (DIC) images of embryonic development. Formaldehyde fixed *C. floridanus* embryos: (**a**) stage 1 (st 1) freshly laid, note the position of the germline capsule primordium (blue arrowhead), (**b**) stage 2 (st 2) nuclear divisions 2-8 (**c**) stage 3 (st 3) nuclear division 9, (**d**) stage 4 (st 4), distinct appearance of the different regions in the embryo; the embryonic region (green arrowheads), and germline capsule (blue arrowhead), (**e**) stage 5 (st 5) cellularization stage, note that the germdisc contains two distinct types of cells embryonic columnar cells and serosal spherical (separated at green arrowhead in e') (**f**) stage 6 (st 6) gastrulation stage, note mesoderm invagination indicated by black arrowhead in f', (**g**) stage 7 (st 7) formation of the germband (green arrowheads), bacteriocytes (magenta arrowhead), putative trophocytes (blue arrow-head in g') and serosa (black arrow-head in g'), (**h**) stage 8 (st 8), elongated germband, (**i**) stage 9 (st 9), fully elongated germband (green arrowheads), note the movement of the bacteriocytes (magenta arrowhead) towards the interior of the egg, uniform appearance of the germband along the AP axis, (**j**) stage 10 (st 10) thickening and patterning of the germband (black arrowheads) (**k**) stage 11 (st 11) appearance of segments (orange arrowheads), orientation of the mouth (black arrowhead) and initiation of germband straightening, (**l**) stage 12 (st 12) straightening of germband, note the gnathal buds first appearance (black arrowhead), (**m**) stage 13 (st 13) initiation of dorsal closure, note the gnathal buds

doi.org/10.32388/OJQCoN

appear more elongated (black arrowheads) (**n**) stage 14 (st 14) rearrangement of head appendages (black arrowheads), (**o**) stage 15 (st 15) completion of dorsal closure, change in positions of gnathal buds (black arrowheads) (**p**) stage 16 (st 16) organogenesis, (**q**) stage 17 (st 17) prelarva, with an intact serosa (black arrowhead). Note the serosa was manually removed in embryos in (**h-p**). Embryos are lateral, dorsal is up and anterior is to the left.

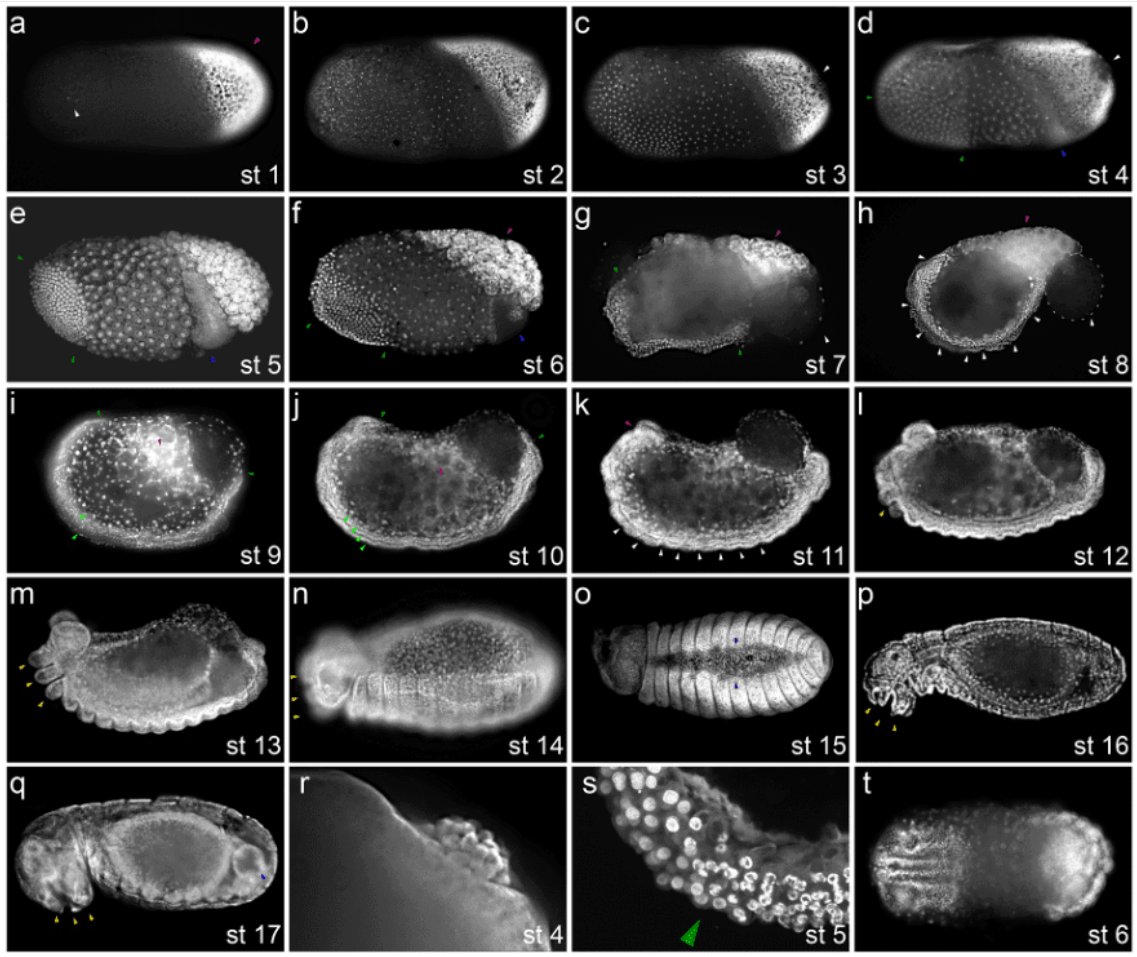

Figure 3. Wide field epifluorescence images of the stages of embryonic development. Nuclear DAPI stained *C. floridanus* embryos: (**a**) stage 1 (st 1) freshly laid, note the zygotic nuclei (white arrowhead) in the anterior and the bacteria in the posterior (bright glow, magenta arrowhead), (**b**) stage 2 (st 2) nuclear divisions 2-8, (**c**) stage 3 (st 3) nuclear division 9 and nuclear migration to periphery note position of pole cells (white arrowhead) (**d**) stage 4 (st 4) distinct appearance of the different zones in the embryo; the embryonic zone (green arrowheads), and germline capsule (blue arrowhead) (**e**) stage 5 (st 5) cellularization stage, (**f**) stage 6 (st 6) gastrulation stage, note the first appearance of complete bacteriocytes (magenta arrowhead), (**g**) stage 7 (st 7) formation of the germband (green arrowheads), (**h**) stage 8 (st 8), elongated germband, note the germline nuclei (white arrowhead) inside the capsule (blue arrowhead) (**i**) stage 9 (st 9), fully elongated germband (green arrowhead), note the movement of the bacteriocytes (magenta arrowhead) towards the interior of the egg, uniform appearance of the germband along the AP axis (white dotted lines) (**j**) stage 10 (st 10) thickening and patterning of the germband (white dotted lines) (**k**) stage 11 (st 11) appearance of segments (white arrowheads), proctodeal invagination (red arrowhead) and initiation of germband straightening, (**l**) stage 12 (st 12) straightening of germband, note the gnathal buds first appearance (yellow arrowhead), (**m**) stage 13 (st 13) initiation of dorsal closure, note the gnathal buds appear more elongated (yellow arrowheads)

doi.org/10.32388/OJQCoN

(**n**) stage 14 (st 14) rearrangement of head appendages (yellow arrowheads), (**o**) stage 15 (st 15) completion of dorsal closure, note the closing gap of the amnion (blue arrowheads) (**p**) stage 16 (st 16) organogenesis, note that the ventral orientation of the mouth (yellow arrowheads), (**q**) stage 17 (st 17) prelarva, (**r**) Tubulin stained stage 4 embryos showing the externalized pole buds, (**s**) The germdisc at stage 5 contains two distinct types of cells; embryonic columnar cells and serosal spherical separated at green arrowhead, (**t**) stage 6 embryo showing the invagination the mesoderm. Note the serosa was removed (g-q). Embryos are lateral oriented dorsal is up with the exception of (o), which is dorsal and (t), which is ventral, anterior is to the left.

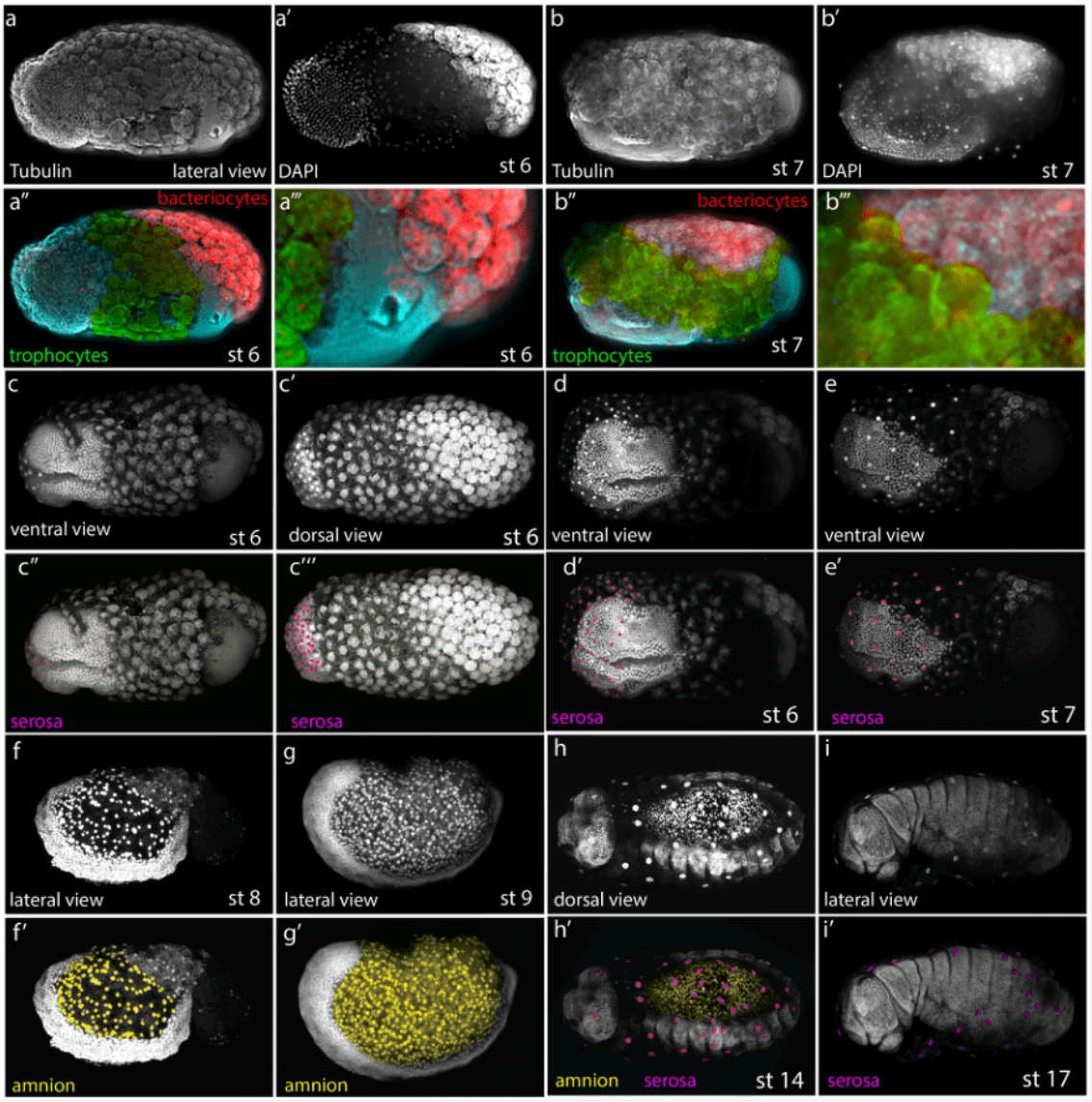

Figure 4. Morphological distinction and spatial distribution of extraembryonic tissues in different embryonic stages. (**a, b**) Confocal scanned images of Tubulin (a,b) and DAPI (a',b') double-stained embryos. Overlaps of the same scans (a", a"', b", b"') highlight the spatial organization of embryonic cells and germline capsule (cyan-Tubulin), putative trophocytes distributed over the middle portion of the egg (green-Tubulin false colored), and bacteriocytes in the dorsal-posterior stongly stained by DAPI (red) due to the presence of endopolyploid bacteria. Tubulin staining reveals a lateral slit adjacent to the cluster of germline nuclei within the germline capsule (a"'). (**c-i**) DAPI stained embryos of different stages. The different stages of serosa expansion are highlighted (false colored magenta) from small spherical cells densely packed at the anterior region (c, c', c", c"') to gradual expansion during stages 6 and 7 (d, e, d', e') and final envelope, which persists till the end of embryogenesis (h, h', i, i'). Different stages of amnion development are highlighted (false colored yellow) from dorsal sheath of the yolk at stage 8 (f, f') to dorsal epithelium of the entire embryo

doi.org/10.32388/OJQCoN

covering the germline capsule and bacteriocytes as well (g, g'), to its detected state before dorsal closure begins in stage 14 (h–h') and absence in the final stage (i, i'). Embryos are oriented lateral with the exception of c, d, e, c", d', e' that are ventral and c', c"', h and h' that are dorsal views. Anterior or to the left.

doi.org/10.32388/OJQCoN

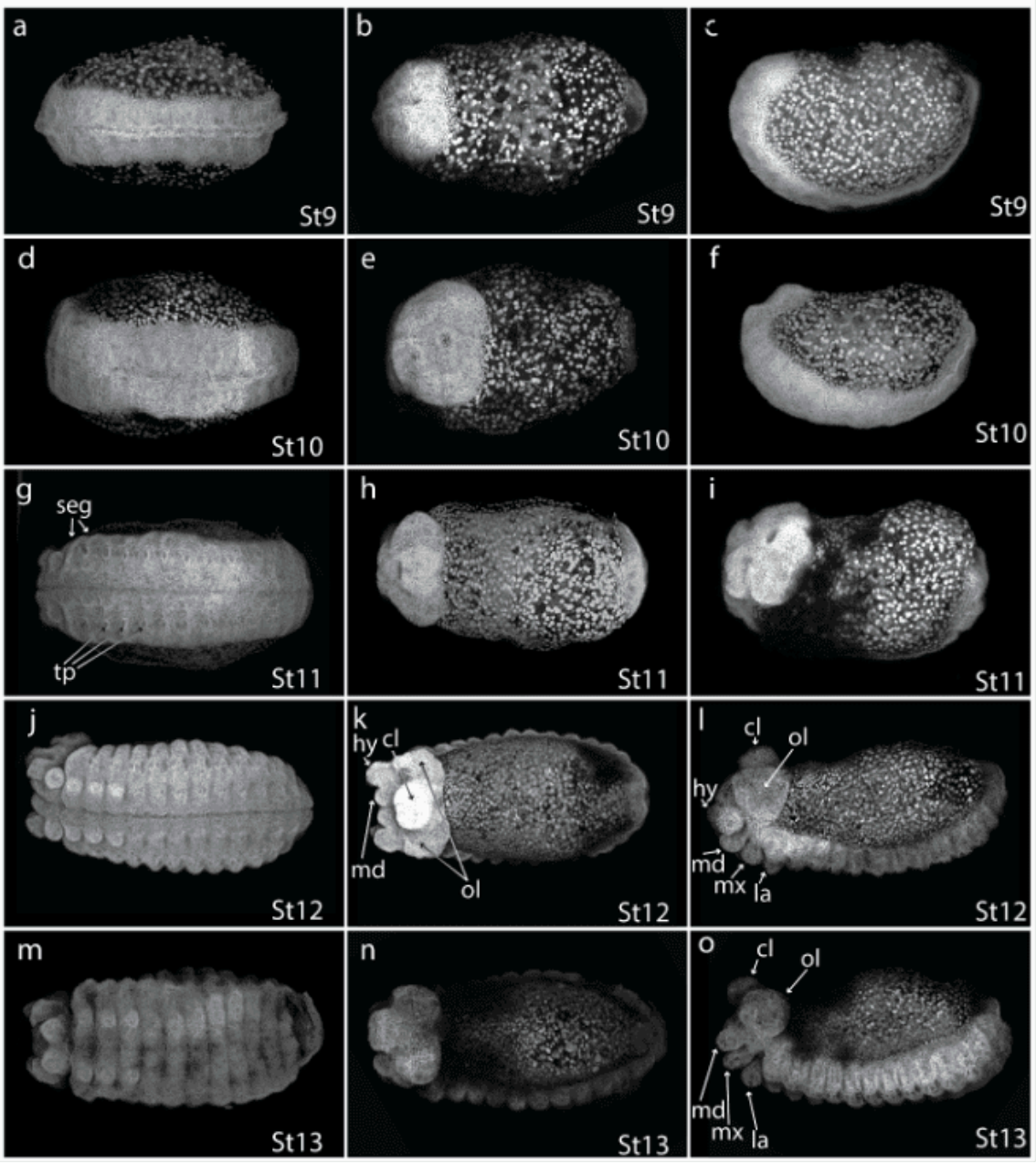

Figure 5. Detailed morphology of later stages *C. floridanus*. (**a-h**) confocal scan maximum projections of DAPI stained embryos of critical stages for embryonic germband and head development. Stage 9 the germband is stretched along the ventral side, extending from the anterior to the posterior pole of the egg (a–c). Stage 10 the head region becomes markedly wider, indicating advanced cephalic development (d-f). Stage 11 the tracheal pits (tp) become visible bilaterally in thoracic segment (seg) T2 through abdominal segment A8 (g–i). Stage 12 cephalic lobes and mouthpart protuberances become more distinct (j–l), the procephalic clypeus (cl) and paired hypopharyngeal lobes (hl), and gnathal buds including the labrum (la), mandibles (md), and maxillae (mx) and optic lobes (ol) are marked. Stage 13 procephalic buds are anterior, and gnathal

doi.org/10.32388/OJQCoN

buds appear more elongated and ventrally oriented (m–o). Embryos in the left column are ventral (a, d, g, j, m), in the middle column are dorsal (b, e, h, k, n), and the right column are lateral (c, f, i, l, o), anterior is to the left.

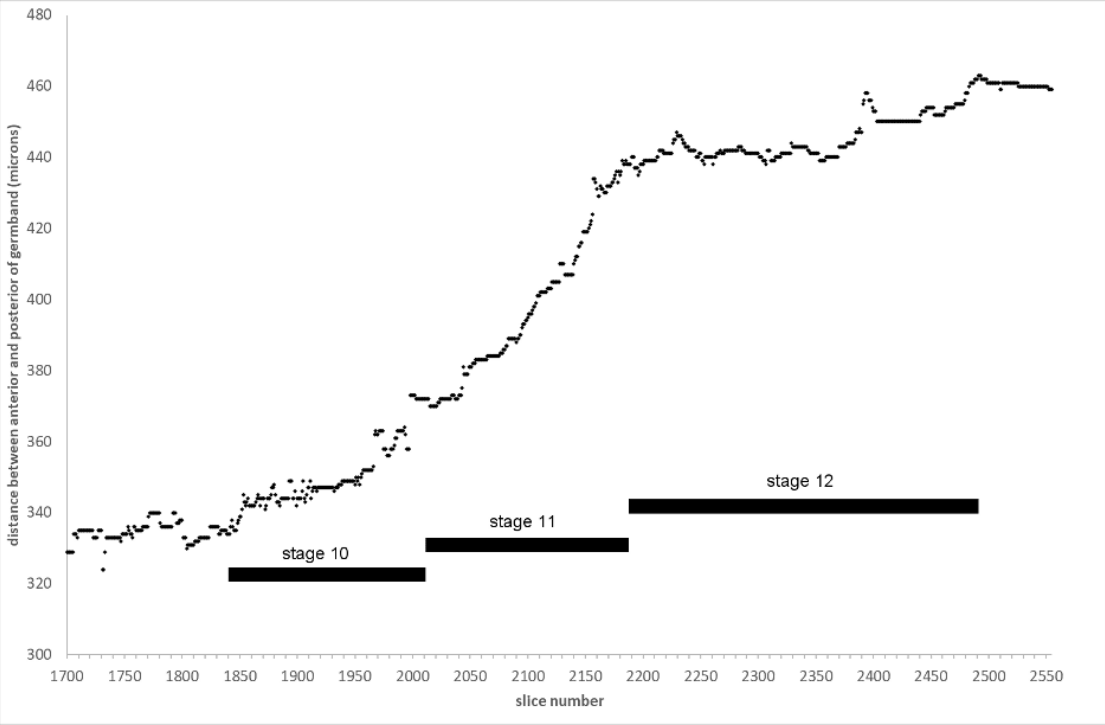

Figure 6. The rate of germband retraction. Measured distance between the anterior and posterior ends of the germband from snapshots of a movie with 5 minute intervals, reflects the progression of germband retraction in three developmental stages. The germband begins to retract or straighten at stage 10, proceeding more rapidly at stage 11, and subsequently slowing down again at stage 12.

doi.org/10.32388/OJQCoN

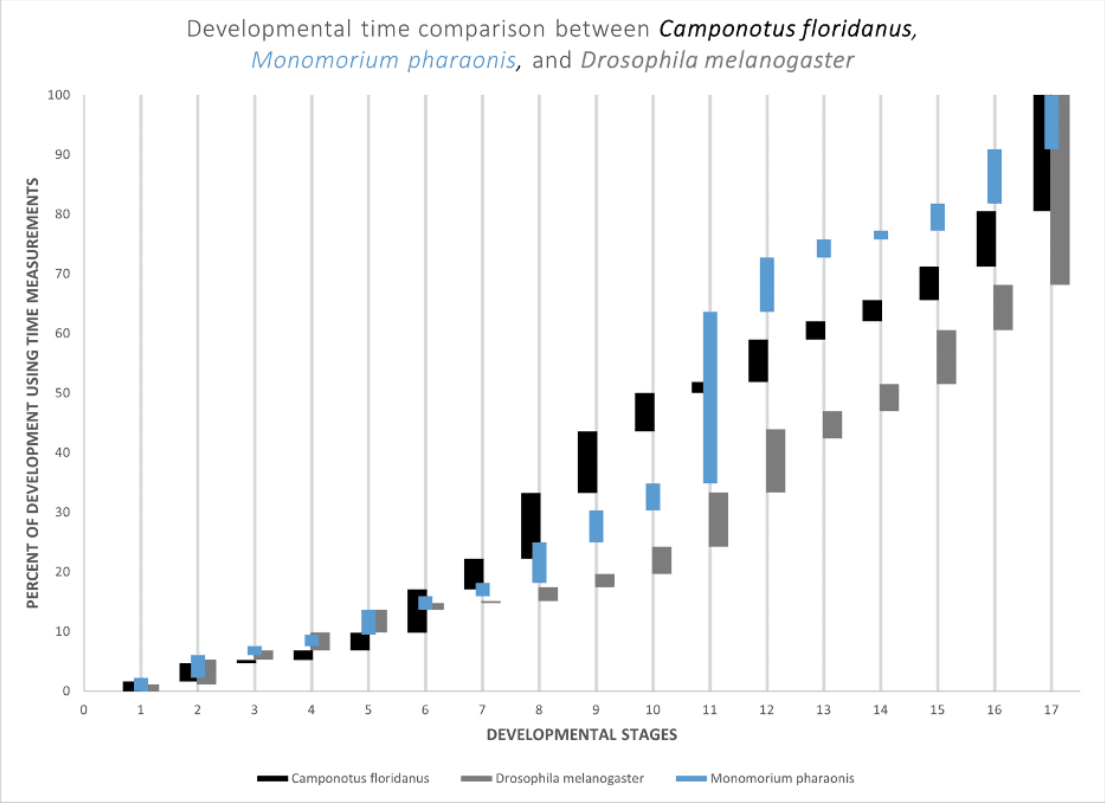

Figure 7. Relative duration of embryonic stages.*C. floridanus* (black bars) in comparison to *M. pharaonis* (blue bars) and *D. melanogaster* (gray bars). Developmental stages are along the X axis, whereas the time taken by each stage as percent of total duration till hatching is represented along the Y axis. *C. floridanus* timing is based on this study, *M. pharaonis* timing is based on[36], *D. melanogaster* timing is based on[27].

doi.org/10.32388/OJQCoN

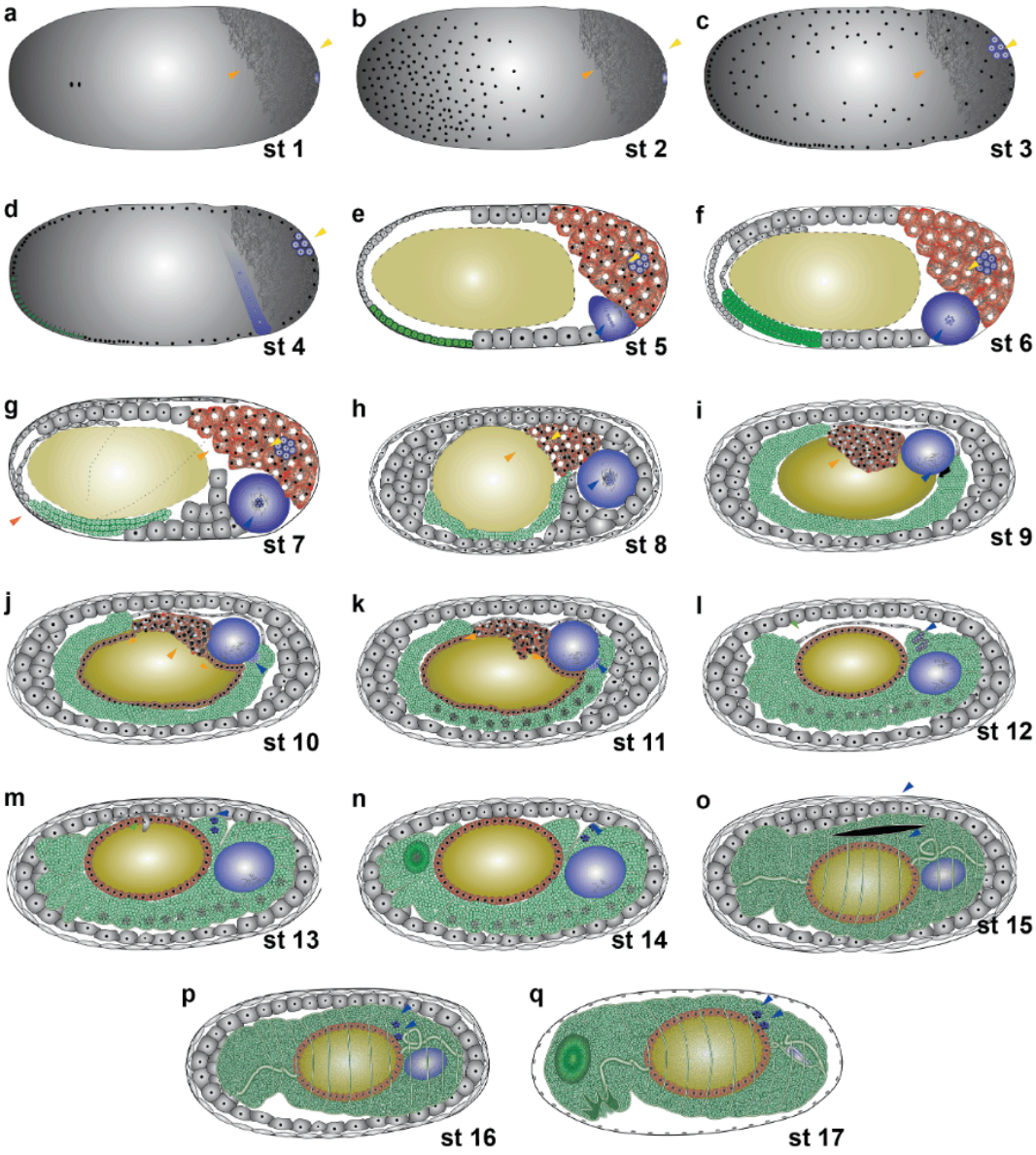

Figure 8. Schematic representation of stages of embryonic development of the C. *floridanus* embryo. (**a-q**) Cartoon representation of stages of embryogenesis. Black circles represent nuclei, and open circles represent cells. Maternal germplasm (a-g), and germline capsule (d-p) are highlighted in blue. Bacteriocytes are highlighted in red (e-q). Bacteria (light orange arrowheads) are shown as rod shapes. Open white circles in bacteriocytes (dark orange arrowheads) represent vacuoles. Note bacteriocytes contain multiple nuclei in earlier stages (e-k) until the nuclei fuse to form single polyploid nucleus (j-q) when lining the midgut periphery. Embryonic cells are colored green and yolk yellow. Note the formation of organized germline nuclei (blue arrowhead) in the germline capsule during stages 6-8 (f-h). The

doi.org/10.32388/OJQCoN

formation of a pair of gonad precursor shown as a pair of dark blue cluster of cells from stages 12 to 17 (l-q). extraembryonic cells are in gray. Anterior is to the right dorsal is up.

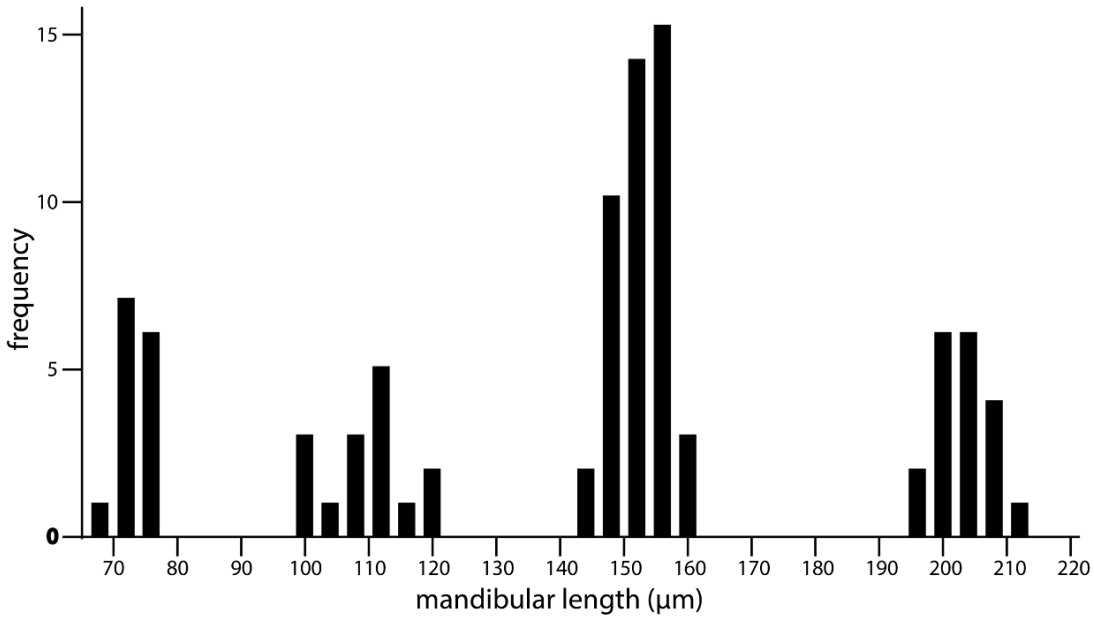

Figure 9. There are 4 larval instars in *C. floridanus* indicated by the frequency distribution of mandibular length of larvae. Histogram of measurements of mandibular length of a random sampling from a colony is shown. Four distinct modal distributions indicate four larval instars.

doi.org/10.32388/OJQCoN

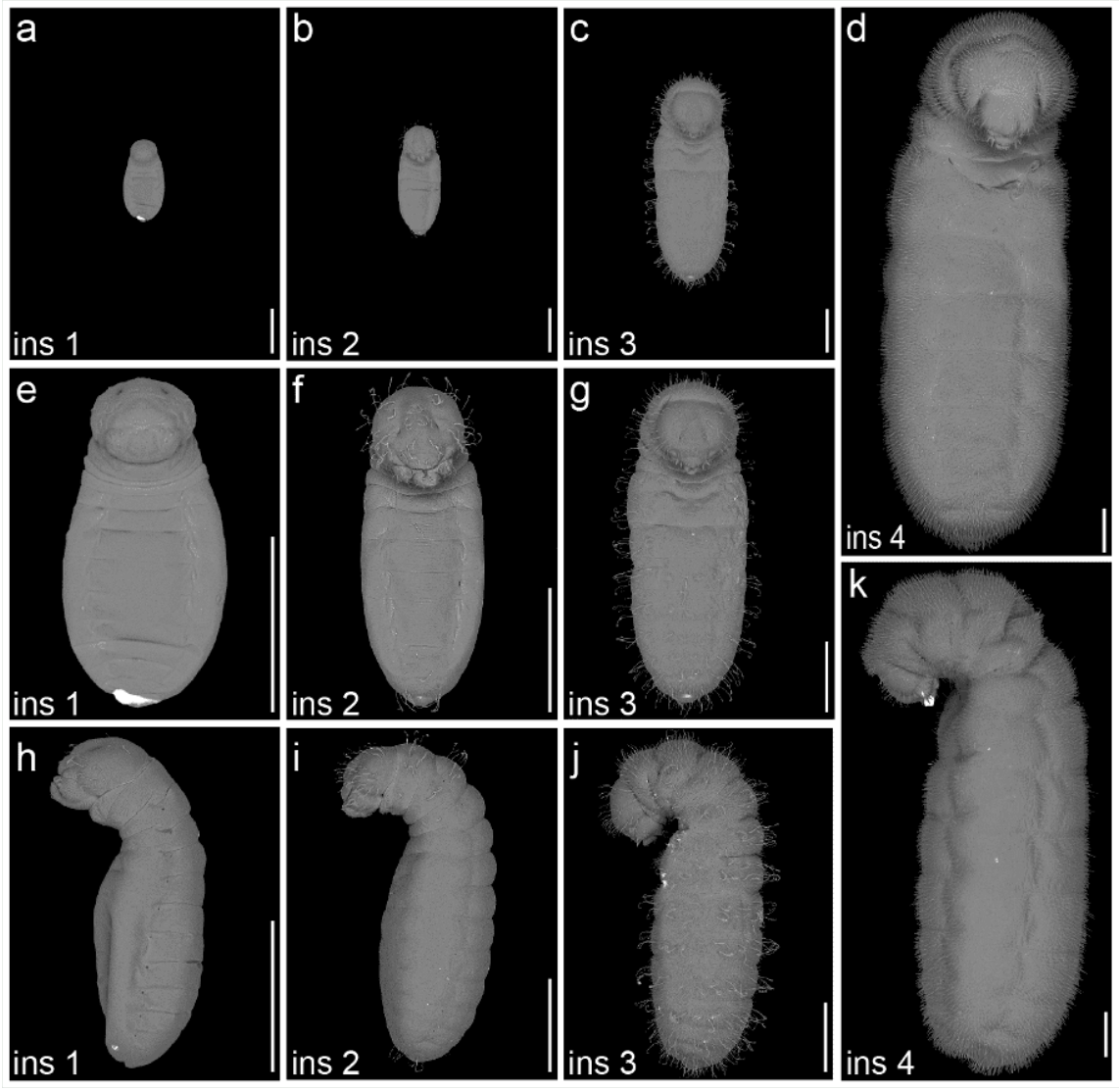

Figure 10. Larval developmental stages. Scanning electron micrograph (SEM) images of the larval instars of *C. floridanus.* (a, e, h) 1st instar larvae, (b, f, i) 2nd instar larvae, (c, g, j) 3rd instar larvae, and (d, k) 4th instar larvae. Note that (d, k) are to scale while other panels have been scaled up. Images were taken from the ventral (a-g) and lateral (h-k) views, anterior is facing up. The scale bar represents 250 µm.

doi.org/10.32388/OJQCoN

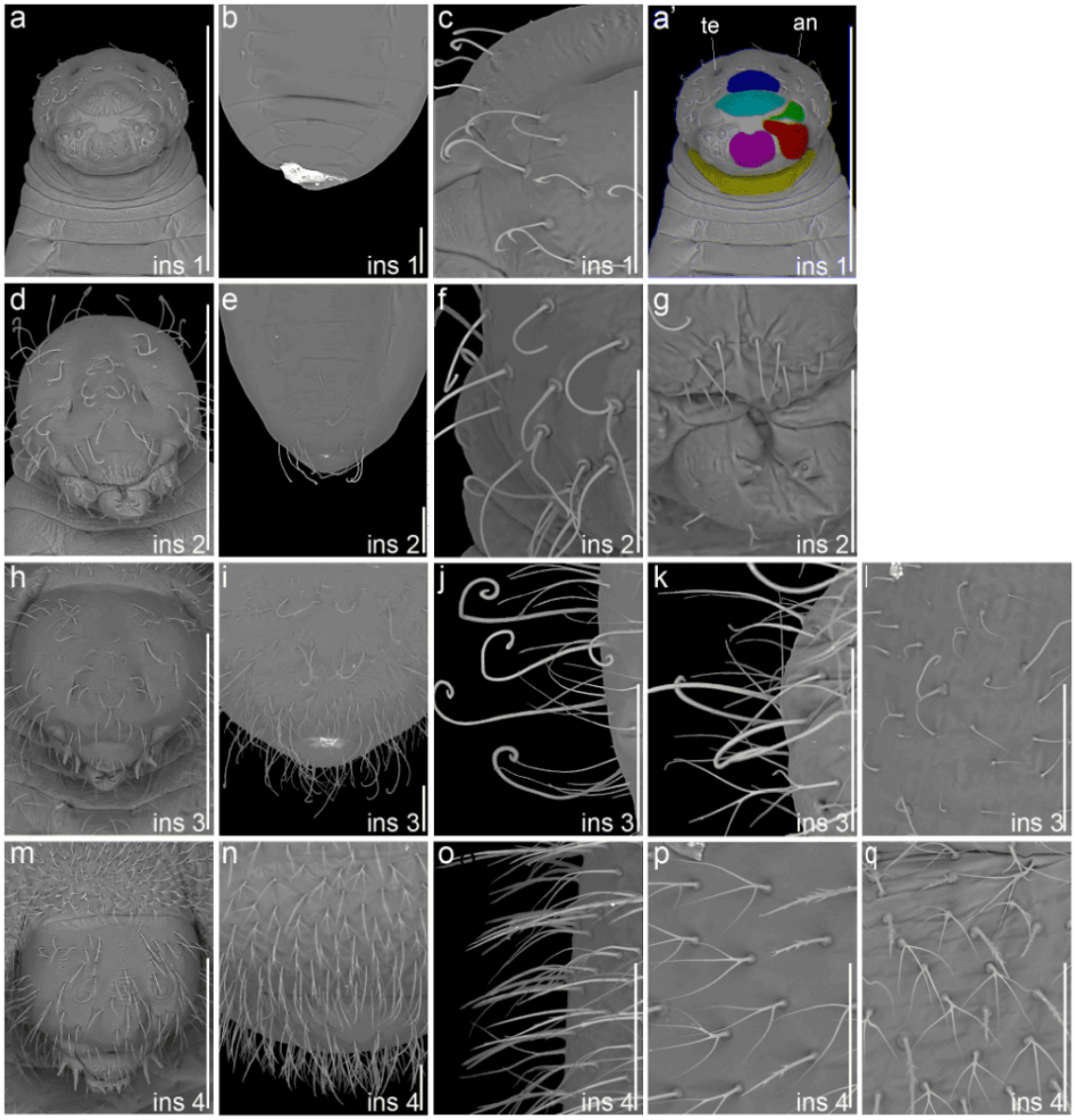

Figure 11. Detailed features of larvae. Scanning electron micrograph (SEM) images of the larval instars of *C. floridanus*. (a-c) 1st instar larvae (ins 1) showing head (a, a'), posterior (b), lateral view of the head (c), (d-g) 2nd instar larvae (ins 2) showing head (d), posterior (e), lateral view of the head (f) and frontal view of the mouth (g), (h-l) 3rd instar larvae (ins 3) showing head (h), posterior (i) and three different types of hairs (j-l), and (m-q) 4th instar larvae (ins 4) showing head (m), posterior (n) and three different types of hairs (o-q) are shown to emphasise the larval hair morphology in detail. False colors in (a') represent the clypeus (blue), labrum (cyan), labium (magenta), mandible (green) maxilla (red), and gula (yellow). 'te' tentorial pit, 'an' antenna. The scale bar represents 250 µm.

doi.org/10.32388/OJQCoN

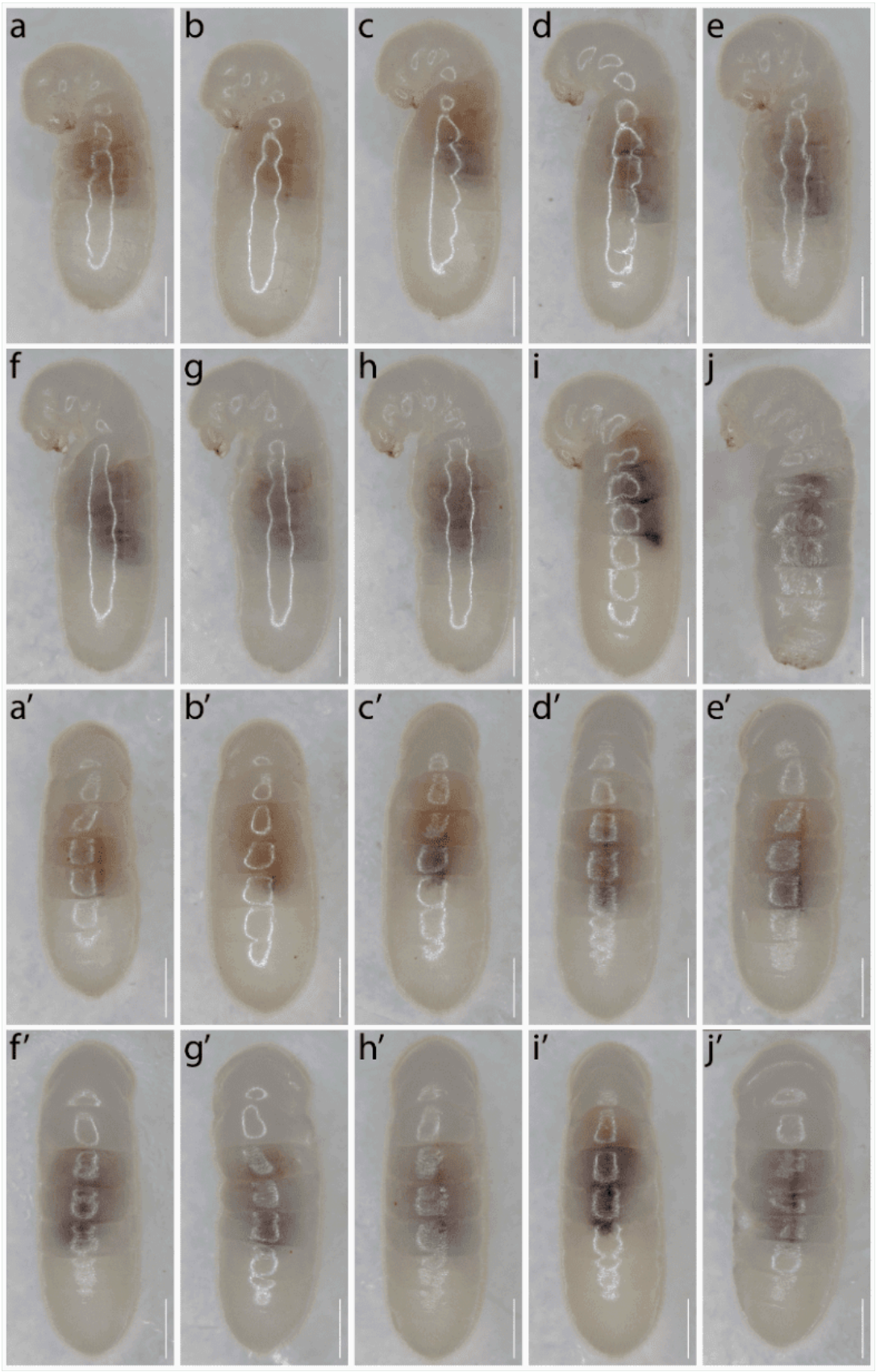

doi.org/10.32388/OJQCoN

Figure 12. Midgut color changes in larvae (a-j) Bright-field images of 4th instar larvae in lateral view showing the changes in the color of their gut with age. (a'-j') bright-field images of the same larvae in dorsal views. Scalebar is 1000 microns.

doi.org/10.32388/OJQCoN

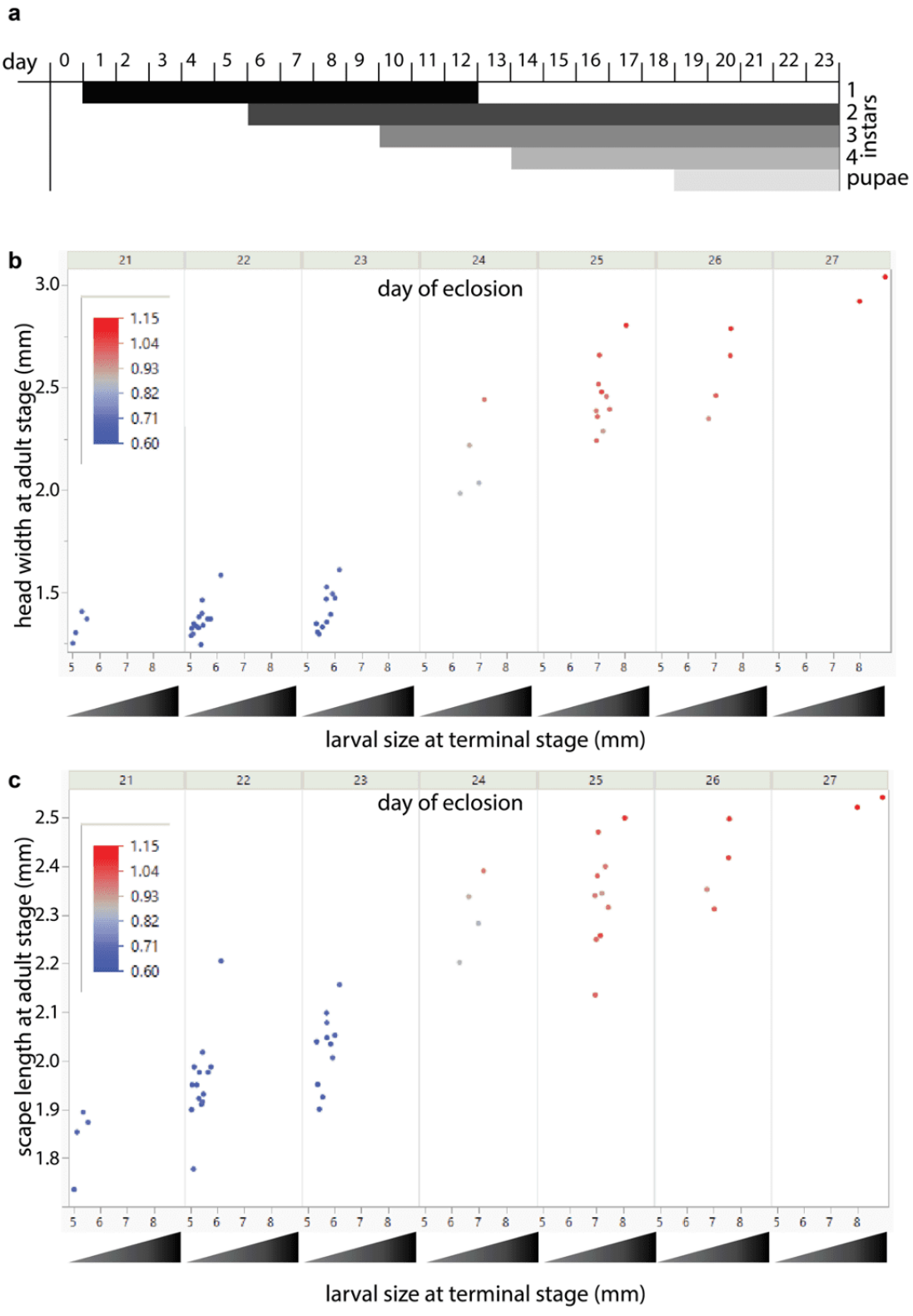

Figure 13. Developmental time and terminal larval size correlate with adult size and allometry (a) Observation of larval instars over days of hatching from embryos **(b)** Correlation of larval size at terminal length (mm) with head width (mm) in the adult. (**c**) Correlation between larval size at terminal length

doi.org/10.32388/OJQCoN

(mm) with scape length (mm) in the adult. Heatmap represents ratio of head width / scape length showing minor workers in blue and soldiers in red. The gray gradient on x-axis represents increasing terminal larval size (mm).

doi.org/10.32388/OJQCoN

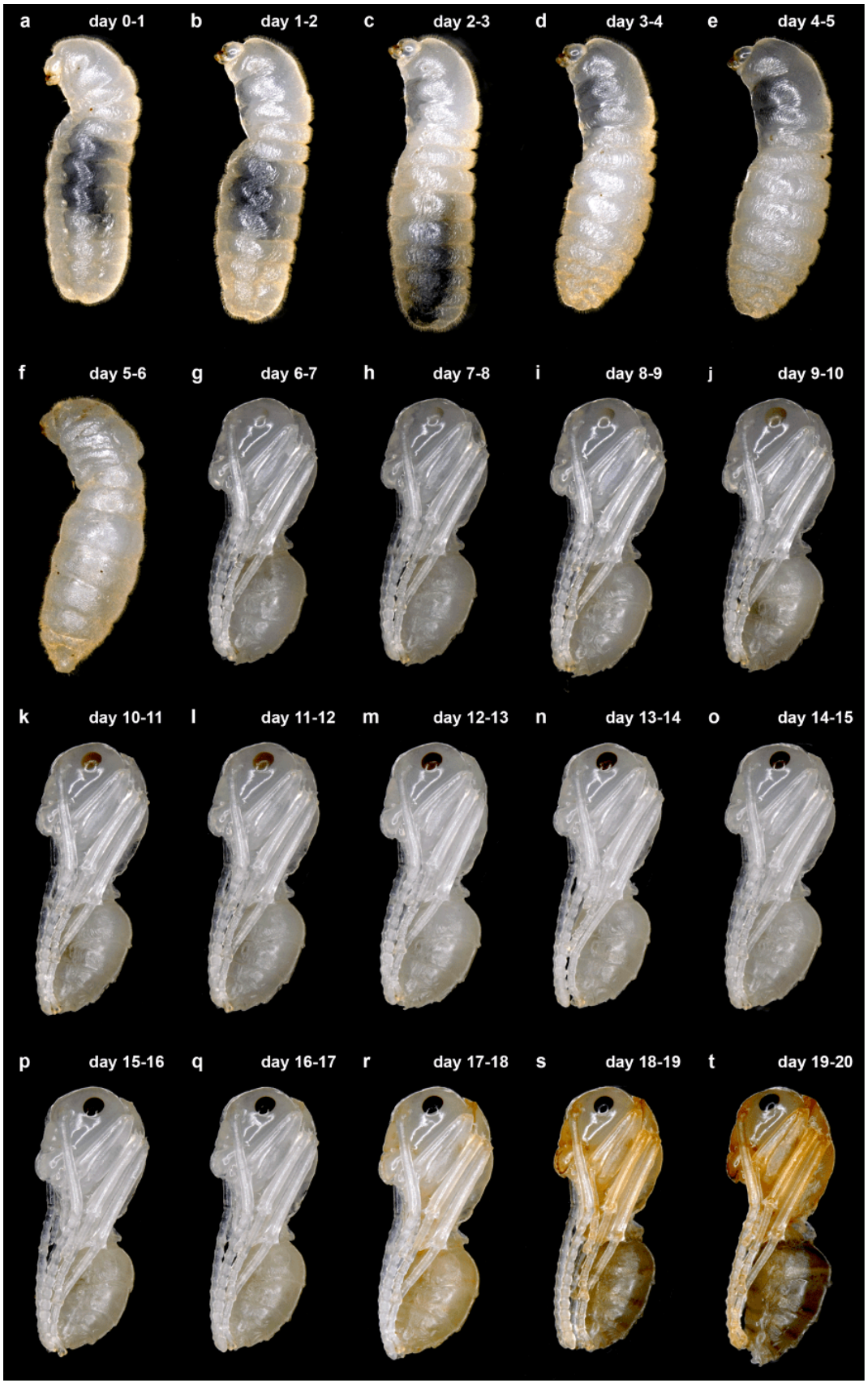

doi.org/10.32388/OJQCoN

Figure 14. Pupal development lateral views. (a-t) Extended focus images of minor worker pupae taken on each day from 0 to 20 days after initiation of pupation. The individuals are size matched at the terminal stage by measuring size and scape length. Time spent since initiation of pupation is indicated as the number of days. Dorsal is to the right, anterior is up.

doi.org/10.32388/OJQCoN

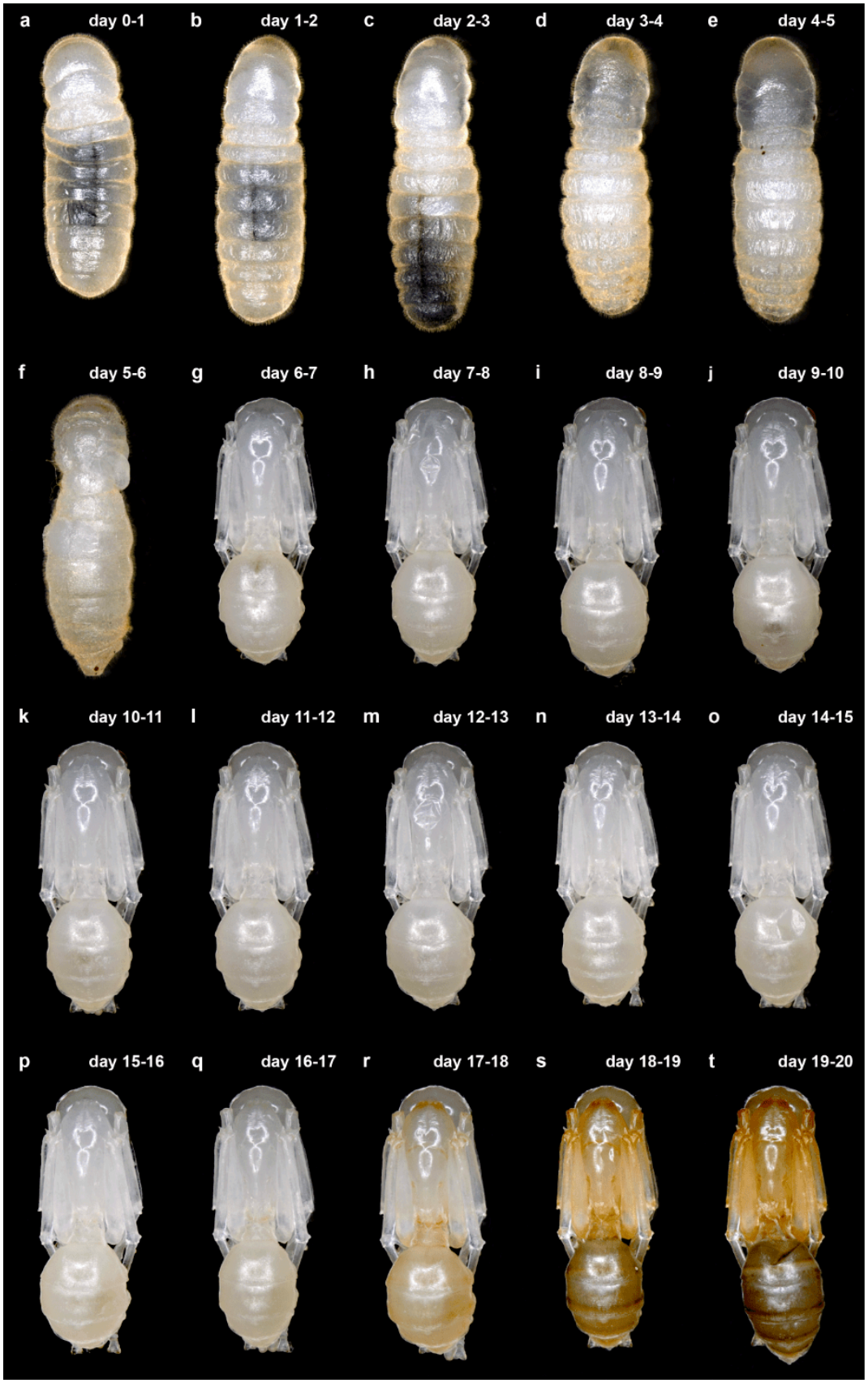

doi.org/10.32388/OJQCoN

Figure 15. Pupal development dorsal views. (a-t) Extended focus images of minor worker pupae taken on each day from 0 to 20 days after initiation of pupation. The individuals are size matched at the terminal stage by measuring size and scape length. Time spent since initiation of pupation is indicated as the number of days. Anterior is up.

doi.org/10.32388/OJQCoN

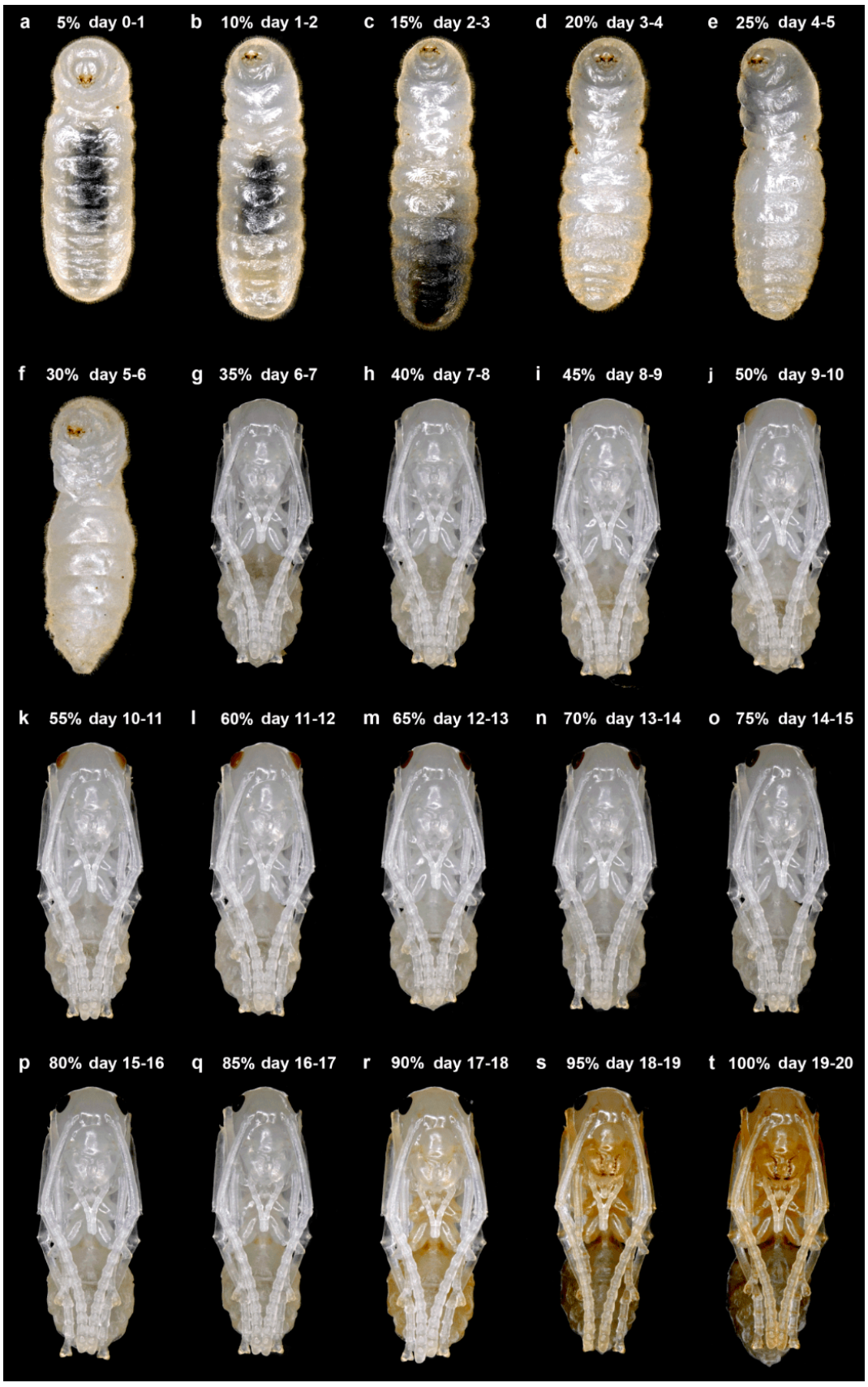

doi.org/10.32388/OJQCoN

Figure 16. Pupal development ventral views. (a-t) Extended focus images of minor worker pupae taken on each day from 0 to 20 days after initiation of pupation. The individuals are size matched at the terminal stage by measuring size and scape length. Time spent since initiation of pupation is indicated as the number of days. Anterior is up.

doi.org/10.32388/OJQCoN

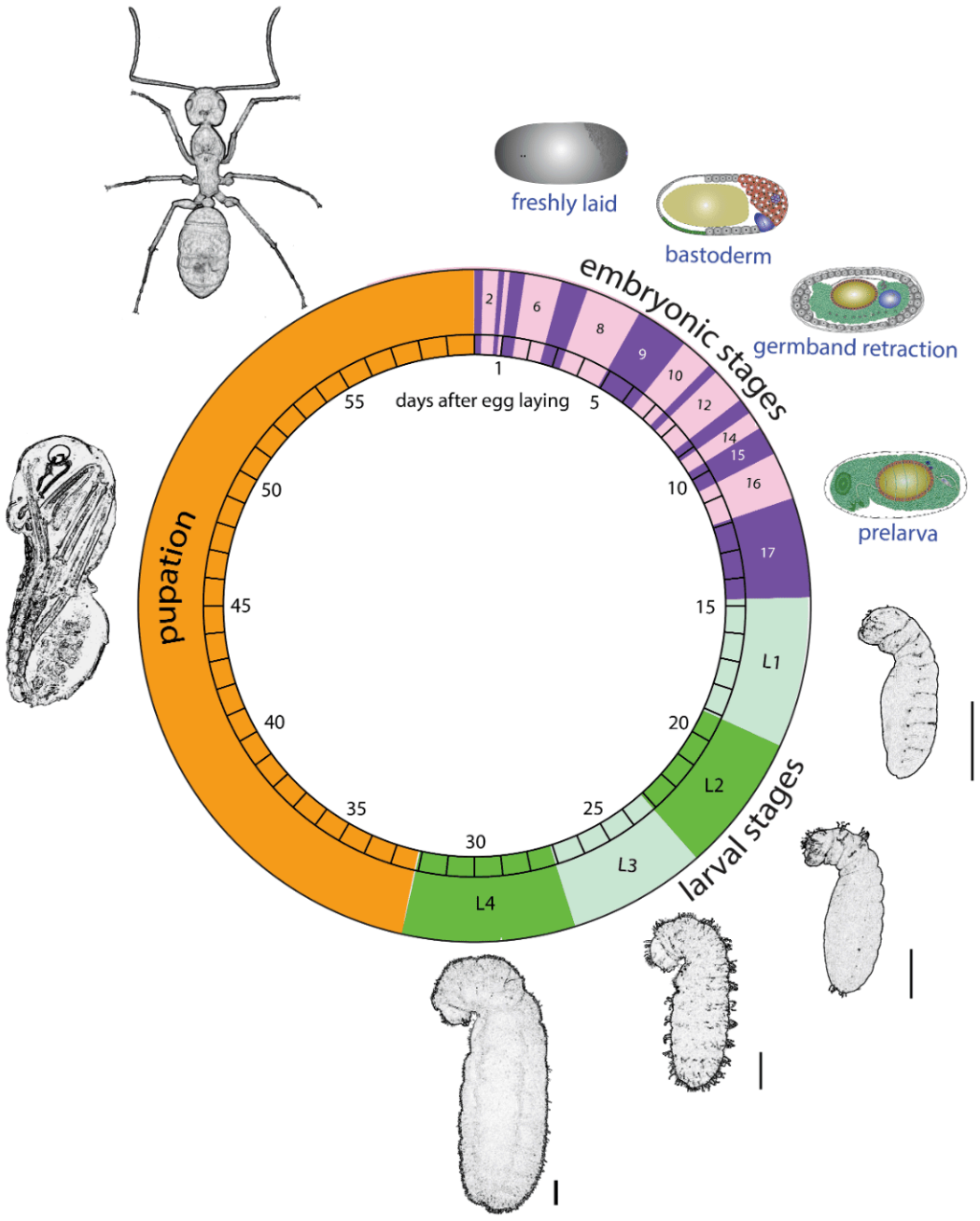

Figure 17. Schematic representation of the development of a worker ant of *C. floridanus*. Embryonic, larval, and pupal stages of *C. floridanus* are shown as arcs of relative length along a circle that represents development from egg laying to adult. Numbers represent the number of days from egg laying. Schematics of important stages are shown outside the circle. Alternative embryonic stages are shown in purple shade, larval stages in green, and pupation in orange color. Embryo cartoons are oriented laterally with anterior to the left, larvae and pupa are oriented laterally with anterior towards the top, while the adult is shown in a dorsal view.

doi.org/10.32388/OJQCoN

Statements and Declarations

Acknowledgements

We would like to thank the Abouheif lab for comments on the manuscript. This work was supported by an NSERC Discovery Grant (Canada) to E.A. and an TÜBİTAK Leader Researcher grant (Turkiye) to A.M.R.

Author contributions

EA, TC, BAF conceived the project. AMR, TC, AR, NSM, TL, EP, BAF, RR performed experiments. AMR, AR, NSM, TC, and BAF performed ant embryonic descriptions and analysis. TC, TL, EP, RR, performed larval descriptions and analysis. TL performed pupal descriptions and analysis. AMR, TC, and EA wrote the manuscript. AMR and TC contributed equally.

References

1. ^*Akam M (1998). "The Yin and Yang of Evo/Devo." Cell. **92**(2):153–155.*
2. ^*Amundson R (2005). The Changing Role of the Embryo in Evolutionary Thought: Roots of Evo-Devo. Cambridge University Press.*
3. ^*de la Rosa LN, Müller GB (2021). Evolutionary Developmental Biology. Springer.*
4. ^*Fusco G (2019). Perspectives on Evolutionary and Developmental Biology. Padova University Press.*
5. ^*Gilbert SF (2003). "The Morphogenesis of Evolutionary Developmental Biology." Int J Dev Biol. **47**(7-8):467.*
6. ^*Moczek AP, Sears KE, Stollewerk A, Wittkopp PJ, Diggle P, Dworkin I, Ledon-Rettig C, Matus DQ, Roth S, Abouheif E (2015). "The Significance and Scope of Evolutionary Developmental Biology: A Vision for the 21st Century." Evol Dev. **17**(3):198–219.*
7. ^*Müller GB (2007). "Evo–Devo: Extending the Evolutionary Synthesis." Nat Rev Genet. **8**(12):943–949.*
8. ^*Raff RA (2000). "Evo-Devo: The Evolution of a New Discipline." Nat Rev Genet. **1**(1):74–79.*
9. ^*Davidson EH, Erwin DH (2010). "Evolutionary Innovation and Stability in Animal Gene Networks." J Exp Zool B Mol Dev Evol. **314**(3):182–186.*
10. ^*Hughes JT, Williams ME, Rebeiz M, Williams TM (2023). "Widespread Cis-and Trans-Regulatory Evolution Underlies the Origin, Diversification, and Loss of a Sexually Dimorphic Fruit Fly Pigmentation Trait." J Exp Zool B Mol Dev Evol. **340**(2):143–161.*

11. ^Lewis EB (1978). "A Gene Complex Controlling Segmentation in Drosophila." Nature. **276**(5688):565–570. doi:10.1038/276565a0.
12. ^Mulhair PO, Holland PW (2024). "Evolution of the Insect Hox Gene Cluster: Comparative Analysis Across 2 43 Species." Semin Cell Dev Biol.
13. ^Rebeiz M, Patel NH, Hinman VF (2015). "Unraveling the Tangled Skein: The Evolution of Transcriptional R egulatory Networks in Development." Annu Rev Genomics Hum Genet. **16**(1):103–131.
14. a, bLevit GS, Hoßfeld U, Naumann B, Lukas P, Olsson L (2022). "The Biogenetic Law and the Gastraea Theor y: From Ernst Haeckel's Discoveries to Contemporary Views." J Exp Zool B Mol Dev Evol. **338**(1-2):13–27.
15. ^Richardson MK (2022). "Theories, Laws, and Models in Evo-Devo." J Exp Zool B Mol Dev Evol. **338**(1-2):36 –61.
16. ^Sander K (1976). "Specification of the Basic Body Pattern in Insect Embryogenesis." Adv Insect Physiol. **12**:1 25–238.
17. ^Slack JM, Holland PW, Graham CF (1993). "The Zootype and the Phylotypic Stage." Nature. **361**(6412):490– 492.
18. ^Duboule D (1994). "Temporal Colinearity and the Phylotypic Progression: A Basis for the Stability of a Vert ebrate Bauplan and the Evolution of Morphologies Through Heterochrony." Development. **1994**(Supplemen t):135–142.
19. ^Kalinka AT, Varga KM, Gerrard DT, Preibisch S, Corcoran DL, Jarrells J, Ohler U, Bergman CM, Tomancak P (2010). "Gene Expression Divergence Recapitulates the Developmental Hourglass Model." Nature. **468**(732 5):811–814.
20. ^Bownes M, Kalthof K (1974). "Embryonic Defects in Drosophila Eggs After Partial U.V. Irradiation at Differe nt Wavelengths." J Embryol Exp Morphol. **31**(2):329.
21. a, b, cFleig R, Sander K (1986). "Embryogenesis of the Honeybee Apis-Mellifera L (Hymenoptera, Apidae) - A n Sem Study." Int J Insect Morphol Embryol. **15**(5-6):449–462. doi:10.1016/0020-7322(86)90037-1.
22. ^Fleig R, Sander K (1988). "Honeybee Morphogenesis - Embryonic-Cell Movements That Shape the Larval Body." Development. **103**(3):525–534.
23. ^Kalthoff K, Sander K (1968). "Der Entwicklungsgang der Mißbildung „Doppelabdomen “im Partiell UV-Bes trahlten Ei von Smittia Parthenogenetica (Dipt., Chironomidae)" [The Development of the Malformation "Double Abdomen" in Partially UV-Irradiated Eggs of Smittia Parthenogenetica (Dipt., Chironomidae)]. Wil helm Roux'Arch Entwicklungsmech Org. **161**(2):129–146.

24. ^Sander K (1968). "Entwicklungsphysiologische Untersuchungen Am Embryonalen Mycetom von Euscelis P lebejus F.(Homoptera, Cicadina): I. Ausschaltung und Abnorme Kombination Einzelner Komponenten des S ymbiontischen Systems" [Developmental Physiological Studies on the Embryonic Mycetome of Euscelis Ple bejus F.(Homoptera, Cicadina): I. Elimination and Abnormal Combination of Individual Components of the Symbiotic System]. Dev Biol. **17**(1):16–38.

25. a, b, cTanquary MC (1912). Biological and Embryological Studies on Formicidae. University of Illinois.

26. ^Brisson JA, Davis GK, Stern DL (2007). "Common Genome-Wide Patterns of Transcript Accumulation Unde rlying the Wing Polyphenism and Polymorphism in the Pea Aphid (Acyrthosiphon Pisum)." Evol Dev. **9**(4):3 38–346.

27. a, b, c, dCampos-Ortega JA, Hartenstein V (2013). The Embryonic Development of Drosophila Melanogaster. Springer Science & Business Media.

28. ^Dearden PK (2006). "Germ Cell Development in the Honeybee (Apis Mellifera); Vasa and Nanos Expressio n." BMC Dev Biol. **6**:6. doi:10.1186/1471-213X-6-6.

29. ^Donoughe S, Extavour CG (2016). "Embryonic Development of the Cricket Gryllus Bimaculatus." Dev Biol. **411**(1):140–156.

30. a, b, c, dFang CC, Rajakumar A, Kenny A, Mueller UG, Abouheif E, Stein D (2025). "Embryogenesis in Myrmici ne Ants Combines Features of Short Germ-Band Development With a Progressive Mode of Segmentation." J Exp Zool B Mol Dev Evol.

31. ^Gainett G, Crawford AR, Klementz BC, So C, Baker CM, Setton EV, Sharma PP (2022). "Eggs to Long-Legs: E mbryonic Staging of the Harvestman Phalangium Opilio (Opiliones), an Emerging Model Arachnid." Front Zool. **19**(1):11.

32. ^Handel K, Grünfelder CG, Roth S, Sander K (2000). "Tribolium Embryogenesis: A Sem Study of Cell Shapes and Movements From Blastoderm to Serosal Closure." Dev Genes Evol. **210**(4):167–179.

33. ^Khila A, Abouheif E, Rowe L (2009). "Evolution of a Novel Appendage Ground Plan in Water Striders Is Dri ven by Changes in the Hox Gene Ultrabithorax." PLoS Genet. **5**(7):e1000583. doi:10.1371/journal.pgen.10005 83.

34. ^Niwa N, Inoue Y, Nozawa A, Saito M, Misumi Y, Ohuchi H, Yoshioka H, Noji S (2000). "Correlation of Diversi ty of Leg Morphology in Gryllus Bimaculatus (Cricket) With Divergence in Dpp Expression Pattern During L eg Development." Development. **127**(20):4373–4381.

35. ^Panfilio KA, Liu PZ, Akam M, Kaufman TC (2006). "Oncopeltus Fasciatus Zen Is Essential for Serosal Tissu e Function in Katatrepsis." Dev Biol. **292**(1):226–243.

36. ^ a b c d e f g h i j k *Rajakumar A, Pontieri L, Li R, Larsen RS, Vásquez-Correa A, Frandsen JK, Rafiqi AM, Zhang G, Abouheif E (2024). "From Egg to Adult: A Developmental Table of the Ant Monomorium Pharaonis." J Exp Zool B Mol Dev Evol. **342**(8):557–585.*

37. ^ *Rosenberg MI, Brent AE, Payre F, Desplan C (2014). "Dual Mode of Embryonic Development Is Highlighted by Expression and Function of Nasonia Pair-Rule Genes." Elife. **3**:e01440.*

38. ^ a b *Antweb (2025). California Academy of Sciences. https://www.antweb.org/.*

39. ^ *Hölldobler B, Wilson EO (1990). The Ants. Harvard University Press.*

40. ^ *Richter A, Economo EP (2023). "The Feeding Apparatus of Ants: An Overview of Structure and Function." Philos Trans R Soc B. **378**(1891):20220556.*

41. ^ *Sosiak CE, Barden P (2021). "Multidimensional Trait Morphology Predicts Ecology Across Ant Lineages." Funct Ecol. **35**(1):139–152.*

42. ^ *Wheeler WM (1910). Ants: Their Structure, Development and Behavior. Columbia University Press.*

43. ^ *Abouheif E, Wray GA (2002). "Evolution of the Gene Network Underlying Wing Polyphenism in Ants." Science. **297**(5579):249–252.*

44. ^ a b c d e f g h i j *Alvarado S, Rajakumar R, Abouheif E, Szyf M (2015). "Epigenetic Variation in the Egfr Gene Generates Quantitative Variation in a Complex Trait in Ants." Nat Commun. **6**:6513. doi:10.1038/ncomms7513.*

45. ^ *Favé MJ, Johnson RA, Cover S, Handschuh S, Metscher BD, Müller GB, Gopalan S, Abouheif E (2015). "Past Climate Change on Sky Islands Drives Novelty in a Core Developmental Gene Network and Its Phenotype." BMC Evol Biol. **15**(1):183.*

46. ^ *Miyazaki S, Murakami T, Kubo T, Azuma N, Higashi S, Miura T (2010). "Ergatoid Queen Development in the Ant Myrmecina Nipponica: Modular and Heterochronic Regulation of Caste Differentiation." Proc R Soc B Biol Sci. **277**(1690):1953–1961.*

47. ^ *Qiu B, Dai X, Li P, Larsen RS, Li R, Price AL, Ding G, Texada MJ, Zhang X, Zuo D (2022). "Canalized Gene Expression During Development Mediates Caste Differentiation in Ants." Nat Ecol Evol. **6**(11):1753–1765.*

48. ^ a b c d e f g h i j k l m *Rafiqi AM, Rajakumar A, Abouheif E (2020). "Origin and Elaboration of a Major Evolutionary Transition in Individuality." Nature. **585**(7824):239–244. doi:10.1038/s41586-020-2653-6.*

49. ^ a b *Rajakumar R, Koch S, Couture M, Favé MJ, Lillico-Ouachour A, Chen T, De Blasis G, Rajakumar A, Ouellette D, Abouheif E (2018). "Social Regulation of a Rudimentary Organ Generates Complex Worker-Caste Systems in Ants." Nature. **562**(7728):574–577.*

50. ^ Rajakumar R, San Mauro D, Dijkstra MB, Huang MH, Wheeler DE, Hiou-Tim F, Khila A, Cournoyea M, Abo uheif E (2012). "Ancestral Developmental Potential Facilitates Parallel Evolution in Ants." Science. **335**(606 4):79–82.

51. ^ Schrader L, Winter M, Errbii M, Delabie J, Oettler J, Gadau J (2021). "Inhibition of Hsp90 Causes Morphologi cal Variation in the Invasive Ant Cardiocondyla Obscurior." J Exp Zool B Mol Dev Evol. **336**(4):333–340.

52. ^ Trible W, Chandra V, Lacy KD, Limón G, McKenzie SK, Olivos-Cisneros L, Arsenault SV, Kronauer DJ (2023). "A Caste Differentiation Mutant Elucidates the Evolution of Socially Parasitic Ants." Curr Biol. **33**(6):1047–10 58.e1044.

53. ^ Yan H, Opachaloemphan C, Carmona-Aldana F, Mancini G, Mlejnek J, Descostes N, Sieriebriennikov B, Leib holz A, Zhou X, Ding L (2022). "Insulin Signaling in the Long-Lived Reproductive Caste of Ants." Science. **37 7**(6610):1092–1099.

54. ^ Yang AS, Abouheif E (2011). "Gynandromorphs as Indicators of Modularity and Evolvability in Ants." J Exp Zool B Mol Dev Evol. **316**(5):313–318.

55. ^ Abouheif E, Favé MJ, Ibarraran-Viniegra AS, Lesoway MP, Rafiqi AM, Rajakumar R (2014). "Eco-Evo-Devo: The Time Has Come." Adv Exp Med Biol. **781**:107–125. doi:10.1007/978-94-007-7347-96.

56. ^ Beldade P, Mateus ARA, Keller RA (2011). "Evolution and Molecular Mechanisms of Adaptive Development al Plasticity." Mol Ecol. **20**(7):1347–1363.

57. ^ Gilbert SF, Bosch TC, Ledón-Rettig C (2015). "Eco-Evo-Devo: Developmental Symbiosis and Developmenta l Plasticity as Evolutionary Agents." Nat Rev Genet. **16**(10):611–622.

58. ^ Gilbert SF, Epel D (2009). Ecological Developmental Biology: Integrating Epigenetics, Medicine, and Evolut ion.

59. ^ Sultan SE (2015). Organism and Environment: Ecological Development, Niche Construction, and Adaptatio n. Oxford: Oxford University Press.

60. ^ Blochmann F (1892). "Uber das Vorkommen Bakterienahnlicher Gebilden in den Geweben und Elem Versc hiedener Insekten" [On the Occurrence of Bacteria-like Structures in the Tissues and Elements of Various In sects]. Zbl Bakteriol. **11**:234–240.

61. ^ Buchner P (1918). "Vergleichende Eistudien 1. Die Akzessorischen Kerne des Hymenoptereneies" [Compara tive Egg Studies 1. The Accessory Nuclei of the Hymenopteran Egg]. Arch Mikrosk Anat. **91**(3-4):1–202.

62. ^ Buchner P (1965). Endosymbiosis of Animals with Plant Microorganisms. Interscience Publishers.

63. ^ Ganin M (1869). Ueber die Embryonalhülle der Hymenopteren-und Lepidopteren-Embryonen [On the Em bryonic Envelope of Hymenopteran and Lepidopteran Embryos]. Vol. 14. Commissionnaires de l'Académie i

mpériale des Sciences.

64. ^*Hegner RW (1914). Studies on Germ Cells: I. The History of the Germ Cells in Insects With Special Reference to the Keimbahn-Determinants. Waverly Press.*

65. ^*Lilienstern M (1932). "Beiträge zur Bakteriensymbiose der Ameisen" [Contributions to the Bacterial Symbiosis of Ants]. Z Morphol Ökol Tiere. **26**(1/2):110–134.*

66. ^*Buckley SB (1866). "Descriptions of New Species of North American Formicidae." Proc Entomol Soc Phila. **6**:152–172.*

67. ^*Mayr G (1861). Die Europäischen Formiciden. Nach der Analytischen Methode Bearbeitet [The European Formicidae. Processed According to the Analytical Method]. C. Gerolds Sohn. http://antcat.org/documents/2123/8104.pdf.*

68. ^*Bolton B (1995). A New General Catalogue of the Ants of the World. Harvard University Press. https://books.google.co.in/books?id=6eh_QgAACAAJ.*

69. ^*Ward PS, Blaimer BB, Fisher BL (2016). "A Revised Phylogenetic Classification of the Ant Subfamily Formicinae (Hymenoptera: Formicidae), With Resurrection of the Genera Colobopsis and Dinomyrmex." Zootaxa. **4072**(3):343–357. doi:10.11646/zootaxa.4072.3.4.*

70. ^a, ^b*Bonasio R, Li Q, Lian J, Mutti NS, Jin L, Zhao H, Zhang P, Wen P, Xiang H, Ding Y, Jin Z, Shen SS, Wang Z, Wang W, Wang J, Berger SL, Liebig J, Zhang G, Reinberg D (2012). "Genome-Wide and Caste-Specific DNA Methylomes of the Ants Camponotus Floridanus and Harpegnathos Saltator." Curr Biol. **22**(19):1755–1764. doi:10.1016/j.cub.2012.07.042.*

71. ^a, ^b, ^c*Bonasio R, Zhang G, Ye C, Mutti NS, Fang X, Qin N, Donahue G, Yang P, Li Q, Li C, Zhang P, Huang Z, Berger SL, Reinberg D, Wang J, Liebig J (2010). "Genomic Comparison of the Ants Camponotus floridanus and Harpegnathos saltator." Science. **329**(5995):1068–1071. doi:10.1126/science.1192428.*

72. ^*Endler A, Liebig J, Schmitt T, Parker JE, Jones GR, Schreier P, Holldobler B (2004). "Surface Hydrocarbons of Queen Eggs Regulate Worker Reproduction in a Social Insect." Proc Natl Acad Sci U S A. **101**(9):2945–2950. doi:10.1073/pnas.0308447101.*

73. ^*Gadau J, Heinze J, Holldobler B, Schmid M (1996). "Population and Colony Structure of the Carpenter Ant Camponotus Floridanus." Mol Ecol. **5**(6):785–792. PMID 8981768.*

74. ^a, ^b*Glastad KM, Graham RJ, Ju L, Roessler J, Brady CM, Berger SL (2020). "Epigenetic Regulator CoREST Controls Social Behavior in Ants." Mol Cell. **77**(2):338–351.e336.*

75. ^a, ^b*Ju L, Glastad KM, Sheng L, Gospocic J, Kingwell CJ, Davidson SM, Kocher SD, Bonasio R, Berger SL (2023). "Hormonal Gatekeeping Via the Blood-Brain Barrier Governs Caste-Specific Behavior in Ants." Cell. **186**(2*

0):4289–4309.e4223.

76. ^*LeBoeuf AC, Waridel P, Brent CS, Goncalves AN, Menin L, Ortiz D, Riba-Grognuz O, Koto A, Soares ZG, Priv man E, Miska EA, Benton R, Keller L (2016). "Oral Transfer of Chemical Cues, Growth Proteins and Hormone s in Social Insects." Elife. **5**. doi:10.7554/eLife.20375.*

77. a, b*Sauer C, Dudaczek D, Holldobler B, Gross R (2002). "Tissue Localization of the Endosymbiotic Bacterium "Candidatus Blochmannia Floridanus" in Adults and Larvae of the Carpenter Ant Camponotus floridanus." Appl Environ Microbiol. **68**(9):4187–4193. doi:10.1128/Aem.68.9.4187-4193.2002.*

78. a, b*Simola DF, Graham RJ, Brady CM, Enzmann BL, Desplan C, Ray A, Zwiebel LJ, Bonasio R, Reinberg D, Lie big J (2016). "Epigenetic (Re)Programming of Caste-Specific Behavior in the Ant Camponotus Floridanus." S cience. **351**(6268):aac6633.*

79. a, b*Simola DF, Ye C, Mutti NS, Dolezal K, Bonasio R, Liebig J, Reinberg D, Berger SL (2013). "A Chromatin Link to Caste Identity in the Carpenter Ant Camponotus floridanus." Genome Res. **23**(3):486–496. doi:10.1101/gr.1 48361.112.*

80. ^*Zube C, Kleineidam CJ, Kirschner S, Neef J, Rossler W (2008). "Organization of the Olfactory Pathway and Odor Processing in the Antennal Lobe of the Ant Camponotus Floridanus." J Comp Neurol. **506**(3):425–441. doi:10.1002/cne.21548.*

81. ^*Straka J, Feldhaar H (2007). "Development of a Chemically Defined Diet for Ants." Insectes Sociaux. **54**(1):1 00–104.*

82. ^*Ratzka C, Gross R, Feldhaar H (2013). "Systemic Gene Knockdown in Camponotus Floridanus Workers by F eeding of DsRNA." Insectes Sociaux. **60**(4):475–484.*

83. ^*Sieriebriennikov B, Reinberg D, Desplan C (2021). "A Molecular Toolkit for Superorganisms." Trends Genet. **37**(9):846–859.*

84. ^*Yan H, Opachaloemphan C, Mancini G, Yang H, Gallitto M, Mlejnek J, Leibholz A, Haight K, Ghaninia M, Hu o L, Perry M, Slone J, Zhou X, Traficante M, Penick CA, Dolezal K, Gokhale K, Stevens K, Fetter-Pruneda I, De splan C (2017). "An Engineered orco Mutation Produces Aberrant Social Behavior and Defective Neural Dev elopment in Ants." Cell. **170**(4):736–747.e739. doi:10.1016/j.cell.2017.06.051.*

85. ^*Smith CD, Zimin A, Holt C, Abouheif E, Benton R, Cash E, Croset V, Currie CR, Elhaik E, Elsik CG (2011). "Dra ft Genome of the Globally Widespread and Invasive Argentine Ant (Linepithema Humile)." Proc Natl Acad S ci U S A. **108**(14):5673–5678.*

86. ^*Smith CR, Smith CD, Robertson HM, Helmkampf M, Zimin A, Yandell M, Holt C, Hu H, Abouheif E, Benton R, Cash E, Croset V, Currie CR, Elhaik E, Elsik CG, Fave MJ, Fernandes V, Gibson JD, Graur D, Gadau J (2011). "D*

raft Genome of the Red Harvester Ant Pogonomyrmex Barbatus." Proc Natl Acad Sci U S A. ***108****(14):5667–5672. doi:10.1073/pnas.1007901108.*

87. ^*Suen G, Teiling C, Li L, Holt C, Abouheif E, Bornberg-Bauer E, Bouffard P, Caldera EJ, Cash E, Cavanaugh A, Denas O, Elhaik E, Fave MJ, Gadau J, Gibson JD, Graur D, Grubbs KJ, Hagen DE, Harkins TT, Currie CR (2011). "The Genome Sequence of the Leaf-Cutter Ant Atta Cephalotes Reveals Insights Into Its Obligate Symbiotic Lifestyle." PLoS Genet.* **7***(2):e1002007. doi:10.1371/journal.pgen.1002007.*

88. ^*Wurm Y, Wang J, Riba-Grognuz O, Corona M, Nygaard S, Hunt BG, Ingram KK, Falquet L, Nipitwattanaphon M, Gotzek D, Dijkstra MB, Oettler J, Comtesse F, Shih CJ, Wu WJ, Yang CC, Thomas J, Beaudoing E, Praderva nd S, Keller L (2011). "The Genome of the Fire Ant Solenopsis Invicta." Proc Natl Acad Sci U S A.* ***108****(14):5679–5684. doi:10.1073/pnas.1009690108.*

89. ^*Agavekar G, Suzuki Y, Suenaga M, Pacheco-Leiva M, Hiller M, Pinto-Tomas AA, Myers E, Economo EP (2025). "A Haplotype-resolved Chromosome-scale Genome Assembly and Annotation for the Leafcutter Ant, Acromyrmex octospinosus." Genome Biol Evol.* ***17****(3). doi:10.1093/gbe/evaf047.*

90. ^*O'Leary NA, Cox E, Holmes JB, Anderson WR, Falk R, Hem V, Tsuchiya MT, Schuler GD, Zhang X, Torcivia J (2024). "Exploring and Retrieving Sequence and Metadata for Species Across the Tree of Life With NCBI Datasets." Sci Data.* ***11****(1):732.*

91. ^*Vizueta J, Xiong Z, Ding G, Larsen RS, Ran H, Gao Q, Stiller J, Dai W, Jiang W, Zhao J, Guo C, Zhang X, Zuo D, Zhong W, Schiøtt M, Liu C, Zhang H, Dai X, Andreu I, Zhang G (2025). "Adaptive Radiation and Social Evolution of the Ants." Cell.* ***188****(18):4828–4848.e4825. doi:10.1016/j.cell.2025.05.030.*

92. ^a, ^b*Bownes M (1975). "A Photographic Study of Development in the Living Embryo of Drosophila Melanogaster." Development.* ***33****(3):789–801.*

93. ^*Sauer C, Stackebrandt E, Gadau J, Hölldobler B, Gross R (2000). "Systematic Relationships and Cospeciation of Bacterial Endosymbionts and Their Carpenter Ant Host Species: Proposal of the New Taxon Candidatus Blochmannia Gen. Nov." Int J Syst Evol Microbiol.* ***50****(5):1877–1886.*

94. ^*Gilbert SF, Barresi M (2016). Developmental Biology, 11th Edit. Sinnauer Associates Inc.*

95. ^*Dahlman DL (1990). "Evaluation of Teratocyte Functions: An Overview." Arch Insect Biochem Physiol.* ***13****(3-4):159–166.*

96. ^*Danyk T, Mackauer M (1996). "An Extraserosal Envelope in Eggs of Praon Pequodorum (Hymenoptera: Aphidiidae), a Parasitoid of Pea Aphid." Biol Control.* ***7****(1):67–70.*

97. ^*Pedata PA, Garonna AP, Zabatta A, Zeppa P, Romani R, Isidoro N (2003). "Development and Morphology of Teratocytes in Encarsia Berlesei and Encarsia Citrina: First Record for Chalcidoidea." J Insect Physiol.* ***49****(1*

1):1063–1071.

98. ^ *Pennacchio F, Vinson S, Tremblay E (1994). "Morphology and Ultrastructure of the Serosal Cells (Teratocyt es) in Cardiochiles Nigriceps Viereck (Hymenoptera: Braconidae) Embryos." Int J Insect Morphol Embryol. **2 3**(2):93–104.*

99. ^ *Rouleux-Bonnin F, Renault S, Rabouille A, Periquet G, Bigot Y (1999). "Free Serosal Cells Originating From t he Embryo of the Wasp Diadromus Pulchellus in the Pupal Body of Parasitized Leek-Moth, Acrolepiosis Ass ectella. Are These Cells Teratocyte-Like?" J Insect Physiol. **45**(5):479–484.*

100. ^ *Strand MR (2014). "Teratocytes and Their Functions in Parasitoids." Curr Opin Insect Sci. **6**:68–73.*

101. ^ *Fang CC, Chang FH, Duong P, Kurian J, Mueller U (2020). "Colony Fitness and Garden Growth in the Asexu al Fungus-Growing Ant Mycocepurus Smithii (Attini, Formicidae)." Insectes Sociaux [Social Insects]. **67**(1):35 –49.*

102. ^ *Nonacs P, Carlin NF (1990). "When Can Ants Discriminate the Sex of Brood? A New Aspect of Queen-Worke r Conflict." Proc Natl Acad Sci U S A. **87**(24):9670–9673. PMID 11607136.*

103. ^ *Stoll S, Feldhaar H, Gross R (2009). "Transcriptional Profiling of the Endosymbiont Blochmannia Floridan us During Different Developmental Stages of Its Holometabolous Ant Host." Environ Microbiol. **11**(4):877–88 8. doi:10.1111/j.1462-2920.2008.01808.x.*

104. ^ *Zientz E, Beyaert I, Gross R, Feldhaar H (2006). "Relevance of the Endosymbiosis of Blochmannia Floridan us and Carpenter Ants at Different Stages of the Life Cycle of the Host." Appl Environ Microbiol. **72**(9):6027– 6033. doi:10.1128/AEM.00933-06.*

105. ^ *Benois A (1972). "Évolution du Couvain et Cycle Annuel de Camponotus Vagus Scop (= Pubescens Fabr.)(H ymenoptera, Formicidae) dans la Région d'Antibes" [Evolution of the Brood and Annual Cycle of Camponot us Vagus Scop (= Pubescens Fabr.)(Hymenoptera, Formicidae) in the Antibes Region]. Ann Zool Ecol Anim [Annals of Animal Zoology and Ecology].*

106. ^ *Bueno O, Rossini S (1986). "Número de Instares Larvais Em Camponotus Rufipes (Fabricius, 1775)(Hymeno ptera, Formicidae)" [Number of Larval Instars in Camponotus Rufipes (Fabricius, 1775)(Hymenoptera, Form icidae)]. Cienc Cult [Science and Culture]. **38**:1009–1010.*

107. ^ *Dartigues D, Passera L (1979). "Larval Polymorphism and the Apparition of Female Castes in Camponotus Aethiops Latreille (Hymenoptera, Formicidae)." Bull Soc Zool Fr [Bulletin of the Zoological Society of Franc e].*

108. ^ a, b, c *Ishii Y, Kubota K, Hara K (2005). "Postembryonic Development of the Mushroom Bodies in the Ant, Ca mponotus japonicus." Zool Sci. **22**(7):743–753, 711. doi:10.2108/zsj.22.743.*

109. ^a, ^bSolis DR, Fox EGP, Kato LM, Jesus CMd, Yabuki AT, Campos AEdC, Bueno OC (2010). "Morphological Description of the Immatures of the Ant, Monomorium Floricola." J Insect Sci. **10**(1):15–15. doi:10.1673/031.010.1501.

110. ^a, ^bSolis DR, Fox EGP, Rossi ML, Bueno OC (2009). "Description of the Immatures of Workers of the Weaver Ant, Camponotus Textor (Hymenoptera: Formicidae)." Sociobiology. **54**(2):541–560.

111. ^Wheeler GC, Wheeler J (1953). "The Ant Larvae of the Subfamily Formicinae." Ann Entomol Soc Am. **46**(1):126–171. doi:10.1093/aesa/46.1.126.

112. ^a, ^bParra JRP, Haddad MdL (1989). Determinação do Número de Ínstares de Insetos [Determination of the Number of Instars of Insects]. Fealq Piracicaba.

113. ^MacMillan O, Singer J, Perrakis S, Craig A, Ntanga D, Qiu D, Rajakumar R (2025). "Juvenile Hormone Signalling Underlies the Switchpoint and Differentiation of Soldiers in Camponotus Floridanus." bioRxiv. 2025.2008.2025.672237.

114. ^Wheeler GC, Wheeler J (1976). Ant Larvae: Review and Synthesis. Washington, DC: Entomological Society of Washington.

115. ^Wheeler DE, Nijhout FH (1981). "Soldier Determination in Ants: New Role for Juvenile Hormone." Science. **213**(4505):361–363.

116. ^Wheeler DE, Nijhout FH (1983). "Soldier Determination in Pheidole Bicarinata: Effect of Methoprene on Caste and Size Within Castes." J Insect Physiol. **29**(11):847–854. doi:10.1016/0022-1910(83)90151-8.

117. ^Wheeler DE, Nijhout FH (1984). "Soldier Determination in Pheidole Bicarinata: Inhibition by Adult Soldiers." J Insect Physiol. **30**(2):127–135. doi:10.1016/0022-1910(84)90116-1.

118. ^Sokolowski MB, Kent C, Wong J (1984). "Drosophila Larval Foraging Behaviour: Developmental Stages." Anim Behav. **32**(3):645–651.

119. ^Gotoh A, Billen J, Hashim R, Ito F (2016). "Degeneration Patterns of the Worker Spermatheca During Morphogenesis in Ants (Hymenoptera: Formicidae)." Evol Dev. **18**(2):96–104.

120. ^Lynch JA, Desplan C (2006). "A Method for Parental RNA Interference in the Wasp Nasonia Vitripennis." Nat Protoc. **1**(1):486–494.

121. ^Lynch JA, Ozuak O, Khila A, Abouheif E, Desplan C, Roth S (2011). "The Phylogenetic Origin of Oskar Coincided With the Origin of Maternally Provisioned Germ Plasm and Pole Cells at the Base of the Holometabola." PLoS Genet. **7**(4):e1002029. doi:10.1371/journal.pgen.1002029.

122. ^Miller SC, Miyata K, Brown SJ, Tomoyasu Y (2012). "Dissecting Systemic RNA Interference in the Red Flour Beetle Tribolium Castaneum: Parameters Affecting the Efficiency of RNAi." PLoS One. **7**(10):e47431.

123. ^ *Bhatkar A, Whitcomb W (1970). "Artificial Diet for Rearing Various Species of Ants." Fla Entomol. :229–232.*

124. ^ *Brady J (1965). "A Simple Technique for Making Very Fine, Durable Dissecting Needles by Sharpening Tung sten Wire Electrolytically." Bull World Health Organ. **32**(1):143.*

125. ^ *Chu DT, Klymkowsky MW (1989). "The Appearance of Acetylated Alpha-Tubulin During Early Developme nt and Cellular Differentiation in Xenopus." Dev Biol. **136**(1):104–117. doi:10.1016/0012-1606(89)90134-6.*

126. ^ *Rueden CT, Schindelin J, Hiner MC, DeZonia BE, Walter AE, Arena ET, Eliceiri KW (2017). "ImageJ2: ImageJ for the Next Generation of Scientific Image Data." BMC Bioinformatics. **18**(1):529. doi:10.1186/s12859-017-193 4-z.*

Supplementary data: available at https://doi.org/10.32388/OJQC0N

Declarations

Funding: NSERC Discovery Grant (Canada) to Ehab Abouheif TÜBİTAK Leader Researcher grant (Turkiye) to Ab. Matteen Rafiqi

Potential competing interests: No potential competing interests to declare.